

Chapter 2

Source of a Tsunami of Seismotectonic Origin

Abstract Modern ideas are presented concerning the source of an earthquake and the seismotectonic source of a tsunami. The main physical processes taking place at a tsunami source are described. Estimation is performed of the role of secondary effects: of displacements of the bottom, occurring in its own plane, of the Coriolis force, of density stratification of the water. The Okada formulae are presented and the technique is exposed for calculating coseismic ocean bottom deformations caused by an underwater earthquake. The dependence of the properties of coseismic ocean bottom deformation at the tsunami source upon the earthquake magnitude and depth is analyzed applying the Okada formulae in the case of a rectangular fault. Formulae are presented that relate the maximum values of the ocean bottom deformation amplitude, the displaced volume, and the initial elevation energy to the moment magnitude of the earthquake. From the slip distribution, adopted from the SRCMOD database, the vector fields of coseismic ocean bottom deformations were calculated applying the Okada formulae for the sources of 75 underwater earthquakes that occurred during the period between 1923 and 2013. It was shown that horizontal deformation components of an inclined bottom, as a rule, provide an additional and noticeable contribution to the displaced water volume and to the potential energy of the initial elevation (the tsunami energy). The relationships were analyzed between the ocean bottom deformation amplitude, the displaced volume and the tsunami energy, and the moment magnitude of the earthquake; the respective regression dependences were plotted. The part of the earthquake energy transferred to the tsunami waves was shown to increase with its moment magnitude, but even in the case of catastrophic earthquakes it does not exceed 0.1 %. From HTDB/WLD and GHTD/NGDC data the peculiarities were investigated of the space–time distribution of tsunamis.

Keywords Tsunami source · Tsunami generation · Bottom earthquake · Moment magnitude · Rectangular fault · Finite fault model · Slip distribution · Coseismic deformation · Initial elevation · Water displacement · Tsunami energy · Tsunami intensity

According to historical data on tsunamis in the World Ocean (HTDB/WLD, GHTD/NGDC) most of the events (more than 70 %) are due to strong underwater earthquakes. In this connection, ideas of the seismotectonic origin of tsunamis are on the

whole certainly of supreme importance for the issue of tsunamis. In this chapter we shall mainly deal with problems of solid-state (-earth) physics, in particular, with problems relevant to the physics of earthquake sources. At the same time, in the first section of this chapter certain hydrodynamic estimates will, nevertheless, be presented, that are necessary for a tsunami-oriented analysis of underwater earthquakes.

2.1 The Main Parameters and Secondary Effects

According to modern ideas, an earthquake is the abrupt release of strain accumulated in the Earth's crust, resulting from the relatively slow motion of lithosphere plates (Kanamori and Brodsky 2004). The source of an earthquake can be represented as a displacement that occurs owing to a fault along one or several planes. In the case of large shallow events the rupture speed amounts to 75–95 % of the velocity of S-waves. An earthquake is characterized by the seismic moment

$$M_0 = \mu DS[\text{N} \cdot \text{m}], \quad (2.1)$$

where μ is the shear modulus of the medium, D is the displacement amplitude between the opposite edges of the fault, S is the area of the fault surface. The earthquake's moment magnitude is related to the seismic moment by the following relationship:

$$M_w = \frac{\log_{10} M_0}{1.5} - 6.07. \quad (2.2)$$

Some seismic events (for example, Sanriku, 1896, the Aleutian earthquake, 1946) caused tsunamis of intensities higher than could be expected from the available seismic data. Kanamori (1972) termed such earthquakes “tsunami earthquakes” and presumed them to occur, when the process at the earthquake source underwent unusually slow development. This case is characterized by a low emission efficiency of the high-frequency component of seismic waves, which is not so important for the process of tsunami generation.

Figure 2.1 presents the relationships between the tsunami intensity (Soloviev–Imamura scale) and the earthquake magnitudes M_S (a) and M_w (b) for the World Ocean constructed by means of the Historical Tsunami Database for the World Ocean (HTDB/WLD) (see Sect. 1.5). The large spread between the data signifies that the relationship between tsunamis and earthquakes is complex and ambiguous. Comparison of the plots presented in Fig. 2.1 permits to conclude that the tsunami intensity dependence upon the magnitude M_S is characterized by a noticeably larger spread than the dependence on the magnitude M_w . The advantage of a moment magnitude scale is quite evident in the case of strong seismic events, which is apparently due to the known saturation problem peculiar to the scale of magnitudes M_S . However, the data spread remains quite significant, also, when the moment magnitude is

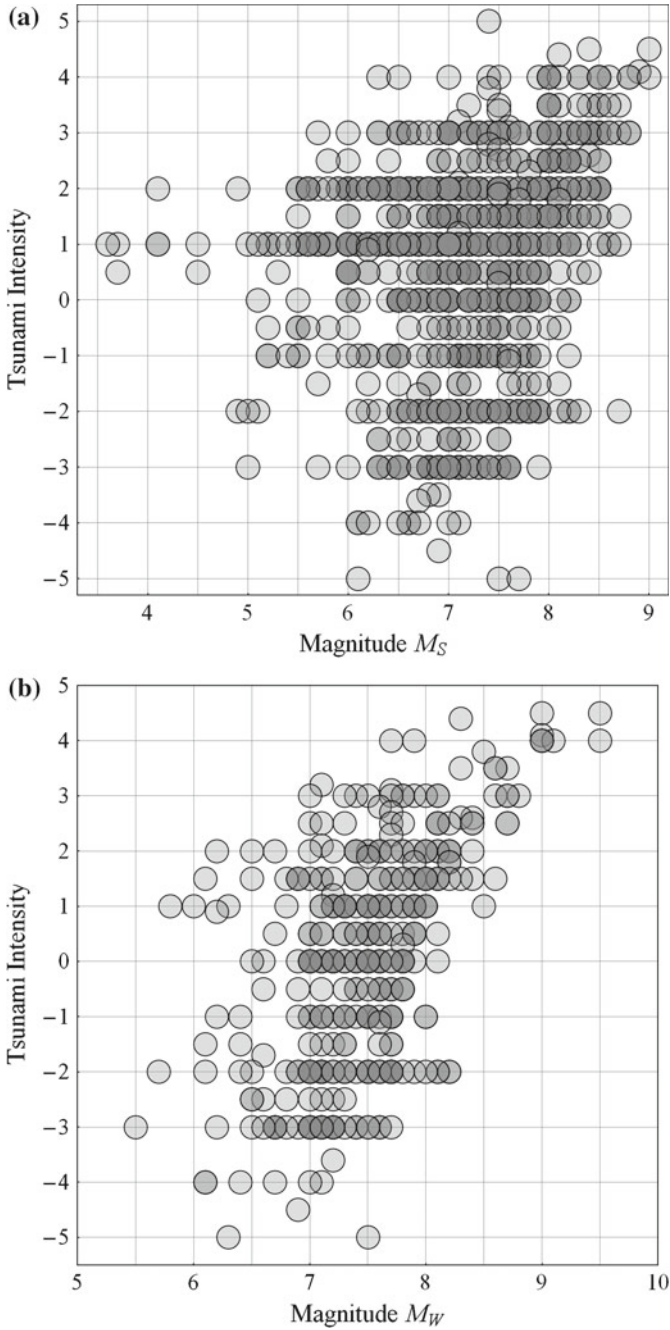


Fig. 2.1 Dependence of the tsunami intensity, according to the Soloviev–Imamura scale, upon the earthquake magnitudes M_S (a) and M_W (b) for the World Ocean

used: if the value of M_w is fixed, the difference in tsunami intensities may differ by several units. For example, if $M_w = 8$, the tsunami intensity varies within 6 units (from -2 up to $+4$). This means that the average heights of tsunami runups may differ by a factor of 64 (2^6)! Hence it becomes evident that a tsunami prognosis based only on seismic data is extremely unreliable. It is also important, here, to note that in the case of strong seismic events the moment magnitude often turns out to be primarily underestimated.

According to Gusiakov (2011) such a significant uncertainty in the tsunami intensity for a fixed earthquake magnitude is due to the following four reasons: (1) the difference in water depths within a source area; (2) the difference in earthquake source mechanisms; (3) the difference in earthquake focus depths; (4) the difference in tectonic settings of the source area (marginal seas, subduction zones, deep-water oceanic plate, etc.).

It is seen that success in the investigation of tsunami generation is related not only to resolution of the hydrodynamic part of the problem, but also to progress in resolving such a difficult problem as description of the earthquake source. It must be noted, that the large spread is also due to the tsunami intensity not being a rigorously defined physical quantity, like, for example, energy. At any rate, a certain positive correlation within the dependences under consideration can be identified: earthquakes of higher magnitudes are generally accompanied by tsunamis of higher intensities. The dependences presented is a good illustration of the magnitude criterion applied in the tsunami warning system. It is seen that the formation of practically all significant tsunamis ($I > 2$) was due to earthquakes of magnitudes $M_w > 7$. Moreover, from Fig. 2.1b one can conclude that earthquakes with magnitudes $M_w \geq 9$ are always accompanied by catastrophic tsunamis of intensities $I \geq 4$.

Figure 2.2 presents distributions of the number of events (tsunamis) over the earthquake source depth and magnitudes M_S (a) and M_w (b). The distributions are based on data from the Historical Tsunami Database for the World Ocean (HTDB/WLD). The HTDB/WLD database contains information on a total of over 2400 tsunamis. The magnitudes M_S and the depths of earthquake sources are known simultaneously for approximately 800 events, while the values of the magnitude M_w and the source depth are known for about 500 events. Most known tsunamis are seen from the figure to originate from strong and shallow earthquakes. The maxima of the distributions lie within the range of magnitudes (M_S or M_w) between 7 and 8 and within the range of source depths from 30 up to 50 km. The rapid decrease in the distributions with the increase of depths and decrease in magnitudes reveals that weak and deep seismic events are rarely accompanied by tsunami waves. The distributions decreasing as the magnitude increases is related to very strong underwater earthquakes occurring extremely rarely, although such seismic events, naturally, always give rise to tsunami waves.

Until the end of the twentieth century, studies of the process of tsunami generation by an earthquake were impeded by the absence of any direct measurements in the source zone. Indeed, all the information on processes proceeding at a tsunami source has been obtained by remote measurements done with mareographs (coastal and deep-water devices), seismographs or hydroacoustic systems. Evidence provided

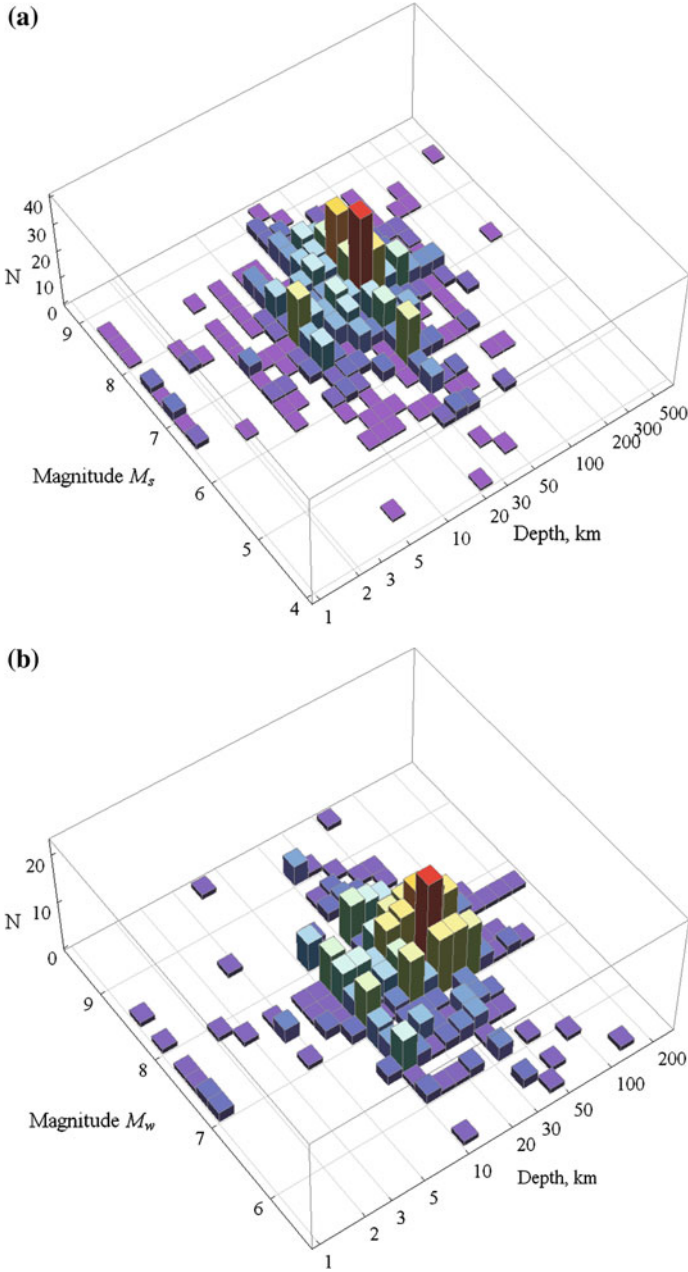


Fig. 2.2 Distributions of the number of events (tsunamis) over the earthquake source depth and magnitudes M_S (a) and M_W (b), based on data from the Historical Tsunami Database for the World Ocean (HTDB/WLD)

by witnesses of underwater earthquakes is quite scarce, and it, naturally, concerns phenomena that took place at the ocean surface. At the beginning of the present century the situation with measurements at a tsunami source changed drastically owing to a sharp rise in the number of deep-water observatories, especially close to Japan. This resulted in the first measurements in history being performed with the aid of sea-bottom stations JAMSTEC (Japan Agency for Marine-Earth Science and Technology) directly at the source of the tsunami Tokachi-Oki of 2003 (Watanabe et al. 2004, Nosov et al. 2005, Mikada et al. 2006). After 7.5 years no less interesting measurements were implemented in 2011 using sea-bottom stations at the source of the catastrophic tsunamigenic earthquake Tokhoku (e.g., Ito et al. 2011).

In simulating a tsunami of seismic origin a convenient method is usually applied that permits not to deal with the description of the generation process in a straightforward manner. The “roundabout maneuver” consists of the following. An earthquake is considered to suddenly cause residual deformations of the ocean bottom (actually the duration of the process at the source may amount to 100 s and more). The residual deformations of the bottom are deduced from the parameters of the earthquake source. Then, the assumption is made that the displacement of the bottom is simultaneously accompanied by formation at the surface of the ocean of a perturbation, the shape of which is fully similar to the residual deformations of the bottom. The perturbation of the water surface (the initial elevation), thus obtained, is then applied as the initial condition in resolving the problem of tsunami propagation.

It is interesting that the possibility to transfer sea-floor perturbations up to the surface is based on the actual structure of the equations for shallow water requiring the sole condition that the sea-floor deformation process be rapid. If, contrariwise, one applies, for instance, potential theory, then, even if the process is instantaneous, the perturbation of the liquid’s surface and the residual deformation will differ from each other.

In general, it is evidently not correct, from a physical point of view, to transfer sea-floor deformations up to the surface. Such an approach turns out to be imperfect, since within its framework at least the following eight factors are neglected: (1) dynamics of the bottom deformation, (2) water compressibility, (3) nonlinear effects, (4) the contribution of horizontal deformations of the sloping (uneven) sea-floor, (5) the smoothing effect of a water layer, (6) stratification, (7) rotation of the Earth, (8) horizontal momentum transfer to the water layer.

The significance of some of the factors mentioned above is quite evident. Thus, for example, in the case of deformation of the seafloor, lasting for a long time, i.e., when a long wave has time to propagate over a noticeable distance, as compared with the horizontal dimension of the source, elevation of the surface will at no particular moment of time coincide with the residual displacements of the seafloor. But this effect could still be taken into account within the framework of the long-wave theory. If, on the other hand, the duration of the deformation is small, then the motion of the water layer must be described within the framework of the theory of a compressible liquid. Here, the theory of long waves turns out to be totally inapplicable. In the case of high-speed displacement of the seafloor an additional contribution to the tsunami wave can also be given by nonlinear effects.

Note the paradoxical effect manifested when tsunami generation is considered as a process proceeding in an incompressible liquid. For definiteness we shall assume an earthquake resulting in area S ($\sqrt{S} \gg H$) of the seafloor being displaced vertically with a constant velocity by a quantity η_0 during a time interval τ . According to the theory of an incompressible liquid, practically all the water layer immediately above the moving part of the seafloor acquires a vertical velocity $\eta_0 \tau^{-1}$, and, consequently, the kinetic energy

$$W_k = \frac{\rho S H \eta_0^2}{2\tau^2}. \quad (2.3)$$

The displacement results in a perturbation forming on the water surface (we shall consider it identical to the deformation of the seafloor), which contains the potential energy

$$W_p = \frac{\rho S g \eta_0^2}{2}. \quad (2.4)$$

The paradox consists in that the kinetic energy involved in the process has a fixed value, but immediately after its completion the kinetic energy disappears without leaving a trace. The paradox is readily resolved, naturally, if the condition $W_p \gg W_k$ is applied. But in reality the kinetic energy may not only be comparable to the potential energy, but even significantly exceed it. Indeed, from formulae (2.3) and (2.4) we have

$$\frac{W_k}{W_p} = \frac{\tau_0^2}{\tau^2},$$

where $\tau_0 = (H/g)^{1/2}$ is the propagation time of a long gravitational wave over a distance equal to the depth of the ocean, ($\tau_0 \approx 20$ s for $H = 4000$ m). In many cases $\tau < \tau_0$, and, consequently, $W_k > W_p$. An accurate resolution of the said paradox is possible within the framework of the theory of compressible liquids.

For an adequate mathematical description of the processes occurring when waves are generated it is necessary to have a clear idea of the characteristic values of the main parameters defining the problem. The range of tsunami wave periods has already been indicated above. The depth of the ocean in area of a tsunami source may vary from several kilometers to zero (when the area of the seafloor deformation extends onto the land). The horizontal size of the tsunami source usually amounts to tens and even hundreds of kilometers. The empirical dependence, that relates the mean radius R_{TS} [km] of the tsunami source and the earthquake magnitude M , is known (Dotsenko and Soloviev 1990a):

$$\lg R_{TS} = (0.50 \pm 0.07) M - (2.1 \pm 0.6). \quad (2.5)$$

Note that real tsunami sources, naturally, do not exhibit a circular, but instead a more complex, as a rule, elongated shape. At any rate, the boundary of a tsunami source is a concept that is essentially conventional. The source of a tsunami of seismic origin can be defined as the area, within which an earthquake has resulted in noticeable residual deformations of the seafloor. From records of waves made by the method of inverse isochrones it is possible to reconstruct the tsunami source region. It is interesting that a source reconstructed in this manner usually exhibits a reasonable correspondence to the area of aftershock manifestations. It must also be stressed that, as a rule, residual deformations are bipolar, i.e., elevation of the seafloor takes place in one part of the source and it is subsided in another part. Figure 2.3, taken from Satake and Imamura (1995), presents the example of the reconstruction of the 1968 Tokachi–Oki tsunami source.

Figure 2.4 shows the areas of the fault surface at the earthquake source (solid line) and of the tsunami source (dotted line) as functions of the earthquake seismic moment (magnitude). The area of the tsunami source was calculated as the area of a circle with a radius determined by formula (2.5). The area of the tsunami source can be seen to be several times larger than the area of the fault at the earthquake source, which is quite reasonable from a physical point of view. It is interesting to note that the said dependencies are practically parallel.

Another essential parameter characterizing tsunami generation by an earthquake is the displacement amplitude ξ_0 [m] of the oceanic surface at the source. This quantity approximately follows the vertical residual deformations of the ocean bottom. The corresponding regression estimate exhibits the following form:

$$\lg \xi_0 = (0.8 \pm 0.1) M - (5.6 \pm 1.0). \quad (2.6)$$

Formulae (2.5) and (2.6) were derived in Dotsenko and Soloviev (1990a) for magnitudes within the range of $6.7 < M < 8.5$ by analysis of the wave field at the source, reconstructed from measurements at the coast. The estimates for intervals correspond to a 80 % probability. Note that formula (2.6) seems to yield overestimated values of residual displacements in the case of large magnitudes. The catastrophic tsunamigenic earthquake, that occurred on December 26, 2004, and the magnitude of which was $M_w = 9.1$, exhibited maximal vertical displacements of 7.8 m for the uplift area and of 5.9 m for the subsidence area (see Fig. 2.15b). Formula (2.6) yields a value ~ 48 m.

The duration of processes at the tsunami source also represents an important parameter of the problem. Here, one must distinguish among several characteristic quantities. Earlier, we already introduced the timescale $\tau_0 = (H/g)^{1/2}$ peculiar to problems involving surface gravitational waves. Besides, there also exists the propagation time of a long gravitational wave over a distance, equal to the horizontal extension of the source, $T_{TS} = R_{TS}(gH)^{-1/2}$. Note that the order of the tsunami wave period depends precisely on the quantity T_{TS} . In a similar manner one can also introduce the propagation time of a hydroacoustic wave along the source, $T_S = R_{TS}/c$, where c is the speed of sound in water. The maximum period of normal elastic oscillations of a water layer, $T_0 = 4H/c$, is also related to hydroacoustic waves. And,

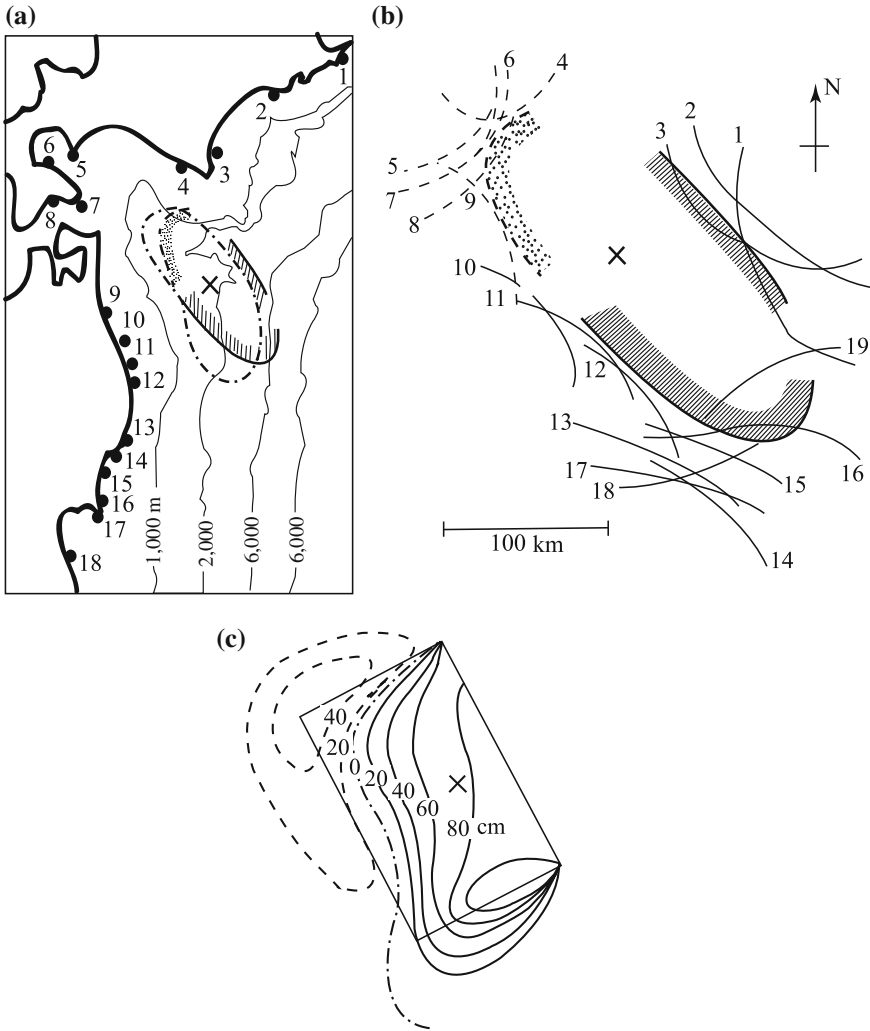


Fig. 2.3 Tsunami source restored applying the method of inverse isochrones (b), and residual deformations of the seafloor (c) for the 1968 Tokachi-Oki earthquake. The figures are the numbers of mareographs, the locations of which are shown in the map (a). The *solid* and *dotted* curves correspond to the positive and negative leading wave, respectively. Adapted from Satake and Imamura (1995)

ultimately, there exists a time, that characterizes the duration of a process occurring at an earthquake source, T_{EQ} . Note that deformation of the seafloor (especially in the case of strong earthquakes) does not proceed simultaneously over the entire area of the tsunami source, but propagates horizontally following the fault that forms at the earthquake source. Therefore, the duration of the seafloor deformation at a

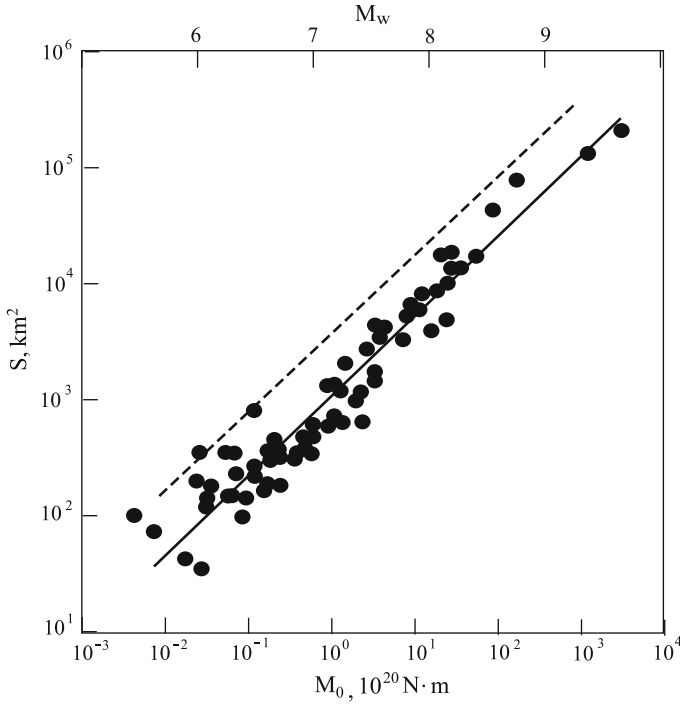


Fig. 2.4 The area of the fault at the source of the earthquake (*solid line*) versus the seismic moment (magnitude). Adapted from Kanamori and Brodsky (2004). The *dotted line* represents an estimation of the area of the tsunami source in accordance with formula (2.3)

certain point may turn out to be significantly shorter than the quantity T_{EQ} . In the Harvard seismic catalogue (<http://www.seismology.harvard.edu/>) a temporal characteristic termed “half duration” is presented, which corresponds to half the duration of the process at an earthquake source. We shall denote this quantity by T_{hd} [s]. Analysis of all the earthquakes of magnitude $M_w > 7$, presented in the Harvard catalogue for the period between January 1976 and March 2005, (370 events) permitted us to obtain the following regression relationship:

$$\lg T_{hd} = (0.42 \pm 0.02) M_w - (1.99 \pm 0.14). \quad (2.7)$$

Such a range of amplitudes was chosen, because significant tsunamis are excited by earthquakes with $M_w > 7$.

Figure 2.5 demonstrates the relation between the above temporal scales and the earthquake magnitude. In constructing the dependences we have applied formulae (2.5) and (2.7) and, besides, for definiteness, we have assumed the ocean depth to vary between 10^2 and 10^4 m.

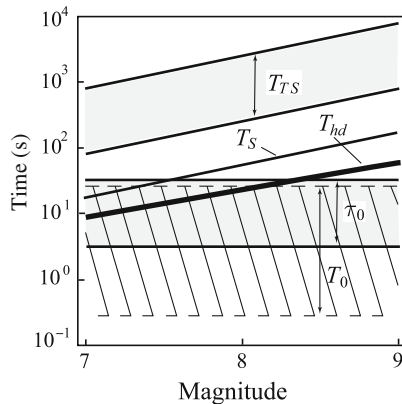


Fig. 2.5 Timescales of a tsunami source as functions of the earthquake magnitude. T_{TS} is the tsunami period, T_{hd} is the duration of the process at the earthquake source (the “half duration”), T_S is the propagation time of the hydroacoustic wave along the tsunami source, T_0 is the maximal period of normal elastic oscillations of the water layer, τ_0 is the timescale for gravitational waves. The ranges correspond to the interval of oceanic depths, 10^2 – 10^4 m

From Fig. 2.5 it can be seen that, as a rule, the duration of processes at the earthquake source, T_{hd} , is significantly inferior to the period of the tsunami wave, T_{TS} , that lies within the range 10^2 – 10^4 s. Therefore, the generation of waves is generally a relatively rapid process. The quantity τ_0 (within the considered range of magnitudes) is always smaller than the period of the tsunami wave, T_{TS} , however, in a number of cases this difference may turn out to be not so significant. In this connection, a tsunami can be considered a long wave, but with certain restrictions: in the case of small-size sources phase dispersion is certain to be manifested. Let us, now, turn to the quantity T_S , which always lies between the quantities T_{TS} and T_{hd} . This reflects the fact that the speed of hydroacoustic waves is always superior to the speed of long waves, but inferior to the speed, with which the fault opens up at the earthquake source. We further turn to elastic oscillations of the water layer. It is readily noted that the quantities T_0 and T_{hd} have very close values, so that effective excitation of elastic oscillations of the water layer is possible at the tsunami source. From the figure it is also seen that the maximal period T_0 of elastic eigen oscillations of the water layer is always smaller than the tsunami period T_{TS} , i.e., elastic oscillations and tsunami waves exist in ranges that do not intersect. This, however, does not mean that elastic oscillations cannot at all contribute to the energy of tsunami waves. Such a contribution can be realized by means of nonlinear effects.

In setting boundary conditions on hard surfaces in hydrodynamic problems one conventionally distinguishes between the normal and tangential components of the flow velocity of the liquid. In the problem of tsunami generation such a hard surface is represented by the ocean bottom, which in the case of an earthquake can undergo motion both in its own plane, and in a perpendicular direction. We will term such displacements tangential and normal. Actually, the surface of the ocean

bottom has a complex structure, therefore the normal is conventionally constructed in a certain plane—the result of averaging either over the entire area of the tsunami source, or over a part of it. We shall consider the differences between this plane and the actual surface of the bottom to be irregularities.

We shall show that, for the excitation of motions in a water layer, normal displacements of the ocean bottom are essentially more effective, than tangential ones. Let each point of the bottom surface at the tsunami source of area S undergo displacement over a distance η_0 during a time τ : once in the tangential direction and then in the normal direction. The normal to the bottom surface is at an angle α to the vertical direction. The slope of the surface of the oceanic bottom rarely exceeds 0.1, therefore the angle α can be considered small.

During tangential shifts the ocean bottom exerts a force on the water layer, equal to $\rho(u^*)^2 S$, where u^* is the friction velocity, ρ is the density of water. The energy transferred to the water layer by the ocean bottom undergoing motion can be estimated as the work performed by this force along the path η_0 :

$$W_t = \rho(u^*)^2 S \eta_0. \quad (2.8)$$

If one passes to the reference frame related to the moving ocean bottom, then one obtains the traditional problem of a logarithmic boundary layer, in which the quantity η_0/τ plays the part of the velocity of the average flow far from the boundary. The friction velocity is known to be essentially smaller than the velocity of the average flow, therefore it is possible to write

$$W_t \ll \rho S \frac{\eta_0^3}{\tau^2}. \quad (2.9)$$

We shall estimate the energy transferred to an incompressible layer of water by a normal displacement as the potential energy of the initial elevation above the water surface. We shall assume the horizontal dimensions of the source to essentially exceed the ocean depth $S^{1/2} \gg H$ and the displacement to be quite rapid, $\tau \ll S^{1/2}(gH)^{-1/2}$. In this case the entire volume of water dislodged by the slip, $\eta_0 S$, will be distributed over an area $S \cos \alpha$ of the ocean surface. Thus, the amplitude of the initial elevation will amount to $\eta_0 / \cos \alpha$. Taking into account the smallness of the angle α we obtain the following estimate for the potential energy of the initial elevation:

$$W_n = \rho g S \frac{\eta_0^2}{2}. \quad (2.10)$$

Let us find the ratio between the energies transferred to the water layer by the normal and tangential displacements,

$$\frac{W_n}{W_t} \gg \frac{g\tau^2}{\eta_0}. \quad (2.11)$$

If one assumes $\eta_0 = \xi_0$, $\tau = T_{\text{hd}}$, and applies formulae (2.6) and (2.7), then one can readily show that $g\tau^2/\eta_0 \approx 800 \gg 1$. Hence it follows that tangential motions of the ocean bottom can be neglected in the problem of tsunami generation.

Thus, movements of the seafloor in a direction perpendicular to the sea bottom surface and accompanied by displacements of water happen to be the main effect leading to tsunami generation.

The real ocean is always stratified, and, moreover, owing to rotation of the Earth each moving particle of the water is under the influence of a Coriolis force. Therefore, tsunami generation is, generally speaking, accompanied by the formation of internal waves and vortical motions.

Let us estimate the effect due to rotation of the Earth, when a tsunami is generated by vertical displacements of the ocean bottom. We shall apply the linearized equations of shallow water written with account of the Coriolis force for a horizontally infinite ocean of depth H .

$$\frac{\partial u}{\partial t} = -g \frac{\partial \xi}{\partial x} + f v, \quad (2.12)$$

$$\frac{\partial v}{\partial t} = -g \frac{\partial \xi}{\partial y} - f u, \quad (2.13)$$

$$H \left(\frac{\partial u}{\partial x} + \frac{\partial v}{\partial y} \right) + \frac{\partial \xi}{\partial t} - \frac{\partial \eta}{\partial t} = 0, \quad (2.14)$$

where u, v are the components of the horizontal flow velocity, $f = 2\omega \sin \varphi$ is the Coriolis parameter, η represents small vertical deformations of the ocean bottom (deviations from the initial position), ξ is the displacement of the free surface from the equilibrium position. We differentiate Eq. (2.12) with respect to the coordinate y and Eq. (2.13) with respect to the coordinate x , and, then, we subtract one from the other. With account of the continuity equation (2.14) we ultimately obtain an evolution equation for the vertical curl component of the velocity

$$\frac{\partial}{\partial t} (\text{rot}_z \mathbf{v}) = \frac{f}{H} \left(\frac{\partial \xi}{\partial t} - \frac{\partial \eta}{\partial t} \right). \quad (2.15)$$

We shall assume no motion to exist in the water layer at the time moment $t = 0$ and the surfaces of the water and ocean bottom to be in an unperturbed state ($\mathbf{v} = 0$, $\eta = 0$, $\xi = 0$). We shall further assume deformation of the ocean bottom, arbitrary in space and time, but quite rapid ($\tau \ll R(gH)^{-1/2}$), to take place within a circular area of radius R , which will result in the formation of certain residual displacements. For simplicity we shall consider the residual displacements to differ from zero only inside the circular area of radius R , where they assume the fixed value η_0 . The ocean bottom displacement results in formation of a wave perturbation of the surface, which after a sufficiently long period of time ($T \gg R(gH)^{-1/2}$) will leave the area of the source and the water surface will return to its initial unperturbed state.

The said assumptions make it possible to integrate Eq. (2.15) over time in the time interval from 0 up to T .

$$(\text{rot}_z \mathbf{v})|_{t=T} = -\frac{f}{H} \eta_0. \quad (2.16)$$

Expression (2.16) permits to conclude that influence of the Earth's rotation manifested at the tsunami source area, considering residual displacements of the ocean bottom to form at the site, must result in formation of a certain vortical structure.

Let us estimate the energy of the vortical structure formed by the circular residual deformation. To this end we integrate expression (2.16) over the area of a circle of radius $r \leq R$, the center of which coincides with the center of the source. Applying the known Stokes formula, we pass in the left-hand part of the obtained expression to circulation of the velocity. With account of the radial symmetry of the problem we obtain, for the velocity of vortical motion at a distance r from the center,

$$V(r) = -\frac{f \eta_0}{2H} \begin{cases} r, & r \leq R, \\ R^2/r, & r > R. \end{cases} \quad (2.17)$$

Knowledge of the velocity distribution readily permits to calculate the kinetic energy of the vortex. However, if the kinetic energy is calculated by integration of the quantity $\rho V^2 H \pi r$ over the radius from 0 up to infinity, then the integral diverges. This result, which at first sight seems paradoxical, is explained as follows. The point is that in deriving formula (2.17) we neglected the residual displacement of the free surface, which is actually peculiar to a vortical structure. Resolving the problem (2.12)–(2.14) carefully yields a velocity decrease, that is more rapid than $1/r$, which provides for convergence of the integral (Nosov and Nurislamova 2012; Nosov et al. 2014).

However, application of formula (2.17) makes it possible to calculate the kinetic energy of the central region of the vortical structure easily. To this end it is sufficient to perform integration from 0 up to R . We shall treat the obtained value as the energy of the vortex resulting from bottom deformation in a rotating ocean:

$$W_k = \frac{\pi \rho f^2 \eta_0^2 R^4}{16 H}. \quad (2.18)$$

Let us, now, compare the energy of the vortex with the energy of the tsunami wave, which we estimate as the potential energy of the initial elevation, similar in shape to the residual deformation of the ocean bottom (a circular area of radius R and height η_0),

$$W_p = \frac{\pi \rho g R^2 \eta_0^2}{2}. \quad (2.19)$$

Comparison of formulae (2.18) and (2.19) reveals the ratio of the energy of the vortex, formed at the tsunami source and due to rotation of the Earth, and the energy of the tsunami wave itself to be given by the following expression:

$$\frac{W_k}{W_p} = \frac{f^2 R^2}{8 g H} \sim 10^{-2} - 10^{-4}. \quad (2.20)$$

The part of the energy due to vortical motion is seen to increase quadratically with the horizontal dimension of the source and to decrease as the ocean depth increases. But, in any case, the contribution of this energy does not exceed 1 % of the energy of the tsunami wave. Note that such an estimate is correct for medium or high latitudes; for equatorial regions, where the Coriolis parameter is small, it will be significantly overestimated.

Let us, now, estimate the energy contribution of internal waves that are due to ocean bottom displacements. We shall consider the model of an ocean consisting of two layers: the upper layer of thickness h_1 with a free surface, and the lower layer of thickness h_2 . The density of the upper layer is ρ_1 and of the lower layer ρ_2 ($\rho_2 > \rho_1$). In this case it is convenient to base estimations on the one-dimensional (along the horizontal coordinate) model, constructed within the framework of the linear theory of long waves. We shall consider a segment of the ocean bottom of length L to undergo a vertical displacement η_0 during a time interval $\tau \ll L (g(h_1 + h_2))^{-1/2}$. Such a displacement represents an impulse not only for surface waves, but also for internal waves, since the propagation velocity of the latter is significantly smaller. The displacement results in the formation of initial elevations both on the water surface and on the boundary surface separating the two layers; we shall consider these elevations to be similar in shape to the deformation of the ocean bottom. In principle, it should be possible already at this stage of reasoning to compare the energies of internal, W_{int} , and of surface, W_{sur} , tsunami waves by comparison of the potential energies of the initial elevations. This ratio is evidently given by the formula

$$\frac{W_{int}}{W_{sur}} \approx \frac{\rho_2 - \rho_1}{\rho_2} \sim 10^{-3}. \quad (2.21)$$

But such a value is actually strongly overestimated. The point is that the evolution of initial elevations gives rise to two sets of waves, each of which consists of perturbations on the water surface and on the jump of density. One of the sets of waves propagates rapidly with the velocity of surface waves, the other one is essentially slower and propagates with the velocity of internal waves. As the initial elevation evolves, the water particles on the free water surface in the vicinity of the source are shifted downward. The maximum of this displacement, equal to η_0 , corresponds to the free surface. At the ocean bottom, owing to there being no flow, the displacement equals zero. Assuming the displacement to depend linearly on the vertical coordinate, we obtain the displacement at the level of the density jump, $\Delta\eta = \eta_0 h_2 / (h_1 + h_2)$. The evolution of the elevation on the free surface is seen to result in the initial elevation at the density jump being reduced by the quantity $\Delta\eta$, while its height becomes

equal to $\eta_{int} = \eta_0 h_1 / (h_1 + h_2)$. Naturally, the potential energy, that is proportional to the square height of the initial elevation, also, decreases, here. A more correct estimation yields the following relationship between the energies of the internal and surface tsunami waves:

$$\frac{W_{int}}{W_{sur}} \approx \frac{\rho_2 - \rho_1}{\rho_2} \left(\frac{h_1}{h_1 + h_2} \right)^2 \sim 10^{-5}. \quad (2.22)$$

Estimations reveal that stratification of the ocean and rotation of the Earth cannot significantly influence the process of tsunami generation by an earthquake. But a small part of the earthquake's energy is transferred both to baroclinic motions and to vortical fields.

A complete physical formulation of the problem of tsunami generation by an earthquake should, generally speaking, consider a layer of viscous compressible stratified liquid on an elastic semispace in the gravitational field with account of the Earth's rotation. The above reasoning makes it possible to essentially simplify formulation of the problem. As a first approximation, we shall consider the process of tsunami generation by an earthquake to be a phenomenon occurring in a homogeneous (nonstratified) perfect incompressible liquid in the gravitational field in an inertial (without rotation) reference frame. Deformations of an absolutely rigid ocean bottom of finite duration and small amplitude ($A \ll H$) serve as the source of waves. Owing to tsunami waves being subject to dispersion, it is expedient to resolve the problem within the framework of potential theory.

In conclusion we shall briefly dwell upon one more possible mechanism of tsunami formation in the case of underwater earthquakes. Experience of the investigation of catastrophic and strong seismic events shows that numerous seismic cracks of lengths exceeding tens of kilometers and widths amounting to 5–15 m arise at the epicentral zone. Dilatant changes of the state of rock in the same area develop, enhancement of the specific volume of the medium takes place, as well as revelation of microcracks and growth of its permeability. In the case of underwater earthquakes such processes should clearly take place in the rock of the ocean bottom. Rapid opening of the cracks at the ocean bottom should lead to an impetuous drainage of water.

Evidence provided by witnesses of the 1999 Izmit earthquake revealed that one of the shallow regions of the Sea of Marmara was dried up by the exclusive drainage of water through cracks in the seafloor; large areas of the seafloor were completely uncovered. In scientific literature, such phenomena are conventionally termed the Moses effect, in memory of the biblical Exodus through the Red Sea. Naturally, the dried areas of the seafloor remain for a short time until the water fills up the entire volume formed by the created set of cracks.

The impetuous drainage of water into cracks results in a local lowering of the ocean level. Such an initial perturbation is also capable of generating tsunami waves. The first results of mathematical simulation of the formation mechanism of a tsunami, caused by a fault opening up in the bottom, are presented in Levin and Nosov (2008).

2.2 Okada Formulae

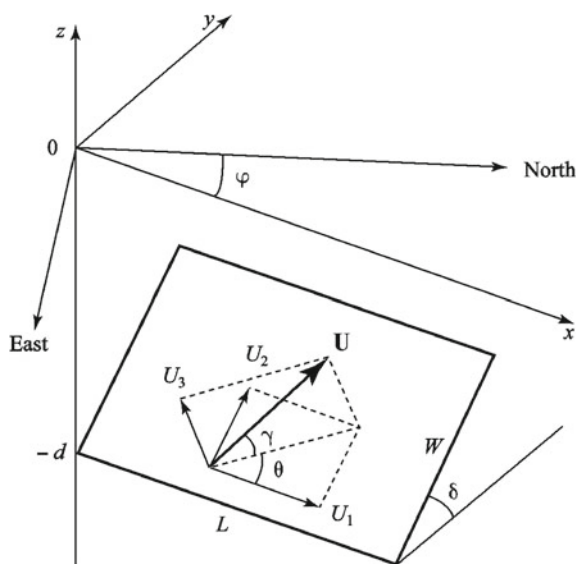
For simulating tsunami waves of seismotectonic origin it is necessary to have realistic data concerning the residual (coseismic or static) deformations of the ocean bottom, resulting from an underwater earthquake. Residual deformations can be calculated on the basis of seismic data, making use of the analytical solution for the stationary problem of elasticity theory. The tensions and displacements caused by sources within the elastic semispace have been studied by many authors (e.g., Chinnery 1961, Maruyama 1964, Press 1965, Savage and Hastie 1966, Gusiakov 1978, Matsu'ura and Tanimoto 1980). In calculations of residual deformations of the ocean bottom at a tsunami source references are usually made to the work of Okada (1985), who brought together, systematized, and checked the calculation formulae carefully. Now these formulae are often termed Okada formulae. It must be stressed that the Okada formulae only permit to calculate static deformations. To reconstruct the dynamics of bottom deformations it is necessary to resolve another, more general, problem.

In this section, formulae are presented for surface displacements due to inclined shear and tensile faults in an isotropic homogeneous elastic half-space. The expressions have been carefully checked to be free from any singularities and misprints.

The Yoshimitsu Okada formulae are quite cumbersome and contain numerous variables. Therefore, in this section, in order to avoid errors, instead of our traditional notation, we shall accurately follow Okada (1985) and apply the original notation adopted therein.

We take the Cartesian reference system as it is shown in Fig. 2.6. The elastic medium occupies the region of $z \leq 0$. The $0x$ axis is taken to be parallel to the strike direction of a finite rectangular fault of length L and width W . Burgers vector

Fig. 2.6 Geometry of the source model (length L , width W , Burgers vector \mathbf{U} , dip angle δ , rake angle θ , angle between Burgers vector \mathbf{U} and the fault plane γ)



$\mathbf{U} = (U_1, U_2, U_3)$ shows the movement of the hanging wall side block relative to the footwall side block. Elementary dislocations U_1 , U_2 , and U_3 are defined so as to correspond to strike-slip, dip-slip, and tensile components of arbitrary dislocations. The tensile component U_3 is normal to the fault plane.

A dislocation is determined by four angles: the strike angle φ (clockwise from North), the dip angle δ , the rake (slip) angle θ , and the angle γ between Burgers vector \mathbf{U} and the fault plane. Elementary dislocations U_1 , U_2 , and U_3 are linked to Burgers vector in the following way: $U_1 = |\mathbf{U}| \cos \gamma \cos \theta$, $U_2 = |\mathbf{U}| \cos \gamma \sin \theta$, $U_3 = |\mathbf{U}| \sin \gamma$.

The final results condensed into compact forms using Chinnery's notation \parallel to represent the substitution

$$f(\xi, \eta) \parallel = f(x, p) - f(x, p - W) - f(x - L, p) + f(x - L, p - W). \quad (2.23)$$

For strike-slip

$$\begin{aligned} u_x &= -\frac{U_1}{2\pi} \left[\frac{\xi q}{R(R + \eta)} + \arctan \left(\frac{\xi \eta}{qR} \right) + I_1 \sin \delta \right] \parallel, \\ u_y &= -\frac{U_1}{2\pi} \left[\frac{\tilde{y}q}{R(R + \eta)} + \frac{q \cos \delta}{R + \eta} + I_2 \sin \delta \right] \parallel, \\ u_z &= -\frac{U_1}{2\pi} \left[\frac{\tilde{d}q}{R(R + \eta)} + \frac{q \sin \delta}{R + \eta} + I_4 \sin \delta \right] \parallel. \end{aligned} \quad (2.24)$$

For dip-slip

$$\begin{aligned} u_x &= -\frac{U_2}{2\pi} \left[\frac{q}{R} - I_3 \sin \delta \cos \delta \right] \parallel, \\ u_y &= -\frac{U_2}{2\pi} \left[\frac{\tilde{y}q}{R(R + \xi)} + \cos \delta \arctan \left(\frac{\xi \eta}{qR} \right) - I_1 \sin \delta \cos \delta \right] \parallel, \\ u_z &= -\frac{U_2}{2\pi} \left[\frac{\tilde{d}q}{R(R + \xi)} + \sin \delta \arctan \left(\frac{\xi \eta}{qR} \right) - I_5 \sin \delta \cos \delta \right] \parallel. \end{aligned} \quad (2.25)$$

For tensile fault

$$\begin{aligned} u_x &= \frac{U_3}{2\pi} \left[\frac{q^2}{R(R + \eta)} - I_3 \sin^2 \delta \right] \parallel, \\ u_y &= \frac{U_3}{2\pi} \left[\frac{-\tilde{d}q}{R(R + \xi)} - \sin \delta \left\{ \frac{\xi q}{R(R + \eta)} - \arctan \left(\frac{\xi \eta}{qR} \right) \right\} - I_1 \sin^2 \delta \right] \parallel, \\ u_z &= \frac{U_3}{2\pi} \left[\frac{\tilde{y}q}{R(R + \xi)} + \cos \delta \left\{ \frac{\xi q}{R(R + \eta)} - \arctan \left(\frac{\xi \eta}{qR} \right) \right\} - I_5 \sin^2 \delta \right] \parallel, \end{aligned} \quad (2.26)$$

where

$$\begin{aligned}
 I_1 &= -\frac{\mu}{\lambda + \mu} \left[\frac{\xi}{(R + \tilde{d}) \cos \delta} \right] - I_5 \tan \delta, \\
 I_2 &= -\frac{\mu}{\lambda + \mu} \ln(R + \eta) - I_3, \\
 I_3 &= \frac{\mu}{\lambda + \mu} \left[\frac{\tilde{y}}{(R + \tilde{d}) \cos \delta} - \ln(R + \eta) \right] + I_4 \tan \delta, \\
 I_4 &= \frac{\mu}{\lambda + \mu} \frac{1}{\cos \delta} \left[\ln(R + \tilde{d}) - \sin \delta \ln(R + \eta) \right], \\
 I_5 &= \frac{\mu}{\lambda + \mu} \frac{2}{\cos \delta} \arctan \left(\frac{\eta(X + q \cos \delta) + X(R + X) \sin \delta}{\xi(R + X) \cos \delta} \right),
 \end{aligned} \tag{2.27}$$

and if $\cos \delta = 0$,

$$\begin{aligned}
 I_1 &= -\frac{\mu}{2(\lambda + \mu)} \frac{\xi q}{(R + \tilde{d})^2}, \\
 I_3 &= \frac{\mu}{2(\lambda + \mu)} \left[\frac{\eta}{R + \tilde{d}} + \frac{\tilde{y} q}{(R + \tilde{d})^2} - \ln(R + \eta) \right], \\
 I_4 &= -\frac{\mu}{\lambda + \mu} \frac{q}{R + \tilde{d}}, \\
 I_5 &= -\frac{\mu}{\lambda + \mu} \frac{\xi \sin \delta}{R + \tilde{d}},
 \end{aligned} \tag{2.28}$$

$$\begin{aligned}
 p &= y \cos \delta + d \sin \delta, \\
 q &= y \sin \delta - d \cos \delta, \\
 \tilde{y} &= \eta \cos \delta + q \sin \delta, \\
 \tilde{d} &= \eta \sin \delta - q \cos \delta, \\
 R^2 &= \xi^2 + \eta^2 + q^2, \\
 X^2 &= \xi^2 + q^2.
 \end{aligned} \tag{2.29}$$

Under special conditions some terms in formulas (2.24)–(2.28) become singular. To avoid all singularities, the following rules should be obeyed:

- i. when $q = 0$, set $\arctan(\xi \eta / q R) = 0$ in Eqs. (2.24)–(2.26);
- ii. when $\xi = 0$, set $I_5 = 0$ in Eq. (2.27);
- iii. when $R + \eta = 0$, set all the terms which contain $R + \eta$ in their denominators to zero in Eqs. (2.24)–(2.28), and replace $\ln(R + \eta)$ by $-\ln(R - \eta)$ in Eqs. (2.27) and (2.28).

To assist the development of a computer program based on expressions (2.23)–(2.29), several numerical results, permitting to check it, are listed in Table 2.1.

Table 2.1 Checklist for numerical calculations

	u_x	u_y	u_z
Case 1: $x = 2$; $y = 3$; $d = 4$; $\delta = 70^\circ$; $L = 3$; $W = 2$			
Strike	$-8.689E - 3$	$-4.298E - 3$	$-2.747E - 3$
Dip	$-4.682E - 3$	$-3.527E - 2$	$-3.564E - 2$
Tensile	$-2.660E - 4$	$+1.056E - 2$	$+3.214E - 3$
Case 2: $x = 0$; $y = 0$; $d = 4$; $\delta = 90^\circ$; $L = 3$; $W = 2$			
Strike	0	$+5.253E - 3$	0
Dip	0	0	0
Tensile	$+1.223E - 2$	0	$-1.606E - 2$
Case 3: $x = 0$; $y = 0$; $d = 4$; $\delta = -90^\circ$; $L = 3$; $W = 2$			
Strike	0	$-1.303E - 3$	0
Dip	0	0	0
Tensile	$+3.507E - 3$	0	$-7.740E - 3$

A medium is assumed to be $\lambda = \mu$ in the all cases, and the results are presented in units of U_i .

When applying Okada formulae in geophysics one should bear in mind that the effect of the Earth's curvature is negligible for shallow events at distances of less than 20° , but that vertical stratification or lateral inhomogeneity can sometimes considerably influence the deformation field. An analysis of the influence exerted on the deformation field by the factors indicated can be found, for example, in Nostro et al. (1999).

The Lamé constants λ and μ enter into expressions (2.27), (2.28) in the form of a combination, which for practical calculations is conveniently expressed via the respective velocities of longitudinal and transverse seismic waves, c_p and c_s ,

$$\kappa \equiv \frac{\mu}{\lambda + \mu} = \frac{c_s^2}{c_p^2 - c_s^2}. \quad (2.30)$$

The following analysis was performed in order to reveal the range of variability of the quantity κ in actual natural conditions. All underwater earthquakes with moment magnitudes $M_w \geq 6$ (about 3600 events during the period of 1976–2012) were selected from the Global CMT Catalog (<http://www.globalcmt.org/>) (Ekström et al. 2012). The quantity κ , we are interested in, was determined for each seismic event from its coordinates and depth in accordance with the global model CRUST2.0 (<http://igppweb.ucsd.edu/~gabi/crust2.html>) (Bassin et al. 2000). It turned out to be that in the case of real underwater earthquakes the quantity κ varies within the range from 0.42 up to 0.52. Variations of the quantity κ within the range indicated weakly affect the result—the residual deformation of the ocean bottom (up to several percent). Therefore, in calculations of residual deformations at tsunami sources the assumption is often made that $\lambda = \mu$, i.e., $\kappa = 0.5$, which, as we see, can be considered quite justified.

2.3 Rectangular Fault: Relationship Between the Parameters of a Tsunami Source and the Earthquake Moment Magnitude and Depth

Many researchers (e.g., Iida 1963, Hatori 1970, Yamashita and Sato 1974, Alekseev and Gusakov 1976, Ward 1980, Kajiura 1981, Dotsenko and Soloviev 1990a, Pelinovsky 1996, Okal 1988, Okal 2003, Bolshakova and Nosov 2011, Poplavskii et al. 2012, Nosov et al. 2014) have been interested in the simple general regularities relating the parameters of a tsunami source and characteristics of the seismic fault area. Usually, in accordance with the approach widely spread in seismology (e.g., Kanamori and Anderson 1975, Kanamori 1977, Sato 1979, Wells and Coppersmith 1994, Okada 1995, Kanamori and Brodsky 2004), attempts were made to relate the parameters of a tsunami source, such as its area (or average radius), the displacement amplitude of the water surface and the initial elevation energy to the earthquake magnitude. In Sect. 2.1, we already presented two such dependences, (2.5) and (2.6), derived from empirical data (Dotsenko and Soloviev 1990b). As another typical example we may note the relation between the tsunami energy (the initial elevation energy) and the magnitude obtained theoretically in Kajiura (1981),

$$\log_{10} E_{TS}[J] = 2.0 M_w - 2.46. \quad (2.31)$$

Making use of the normal mode theory (Okal 2003) analytically obtained an expression relating the tsunami energy within a distant zone to the seismic moment M_0 (dyn \times cm):

$$E_{TS}[\text{ergs}] = 7.4 \times 10^{-17} M_0^{4/3}. \quad (2.32)$$

Passing in formula (2.32) to SI units and expressing the seismic moment via the moment magnitude by means of formula (2.2), formula (2.32) is readily rewritten in terms of the momentary magnitude:

$$\log_{10} E_{TS}[J] = 2.0 M_w - 1.66. \quad (2.33)$$

It is remarkable that in spite of the difference between the approaches applied for obtaining expressions (2.31) and (2.33) they demonstrate an impressive similarity. However, Kajiura's formula (2.31) yields energy values that are underestimated by a factor of approximately 6.3 in comparison to Okal's formula (2.33). What concerns the accuracy of theoretical estimates of the tsunami energy, as noted by Okal himself (2003), there regretfully exist no experimental methods permitting to measure the energy of large transoceanic tsunamis. It may be that the only more or less reliable method for estimating the energy of a tsunami consists in calculating the potential energy of initial elevation.

The interest in general relationships such as (2.5), (2.6), (2.31)–(2.33) is readily explained. They can turn out to be useful not only for operative estimation of an earthquake tsunamigenicity, but also from the point of view of understanding the physical nature of phenomena taking place in the water layer above the underwater earthquake source. On the basis of such relationships, for example, it is possible, from the given earthquake magnitude and depth, to rapidly estimate the maximum possible amplitude of waves at the source, as well as their length, to determine the part of the earthquake energy transferred to the tsunami wave or to some other dynamic process.

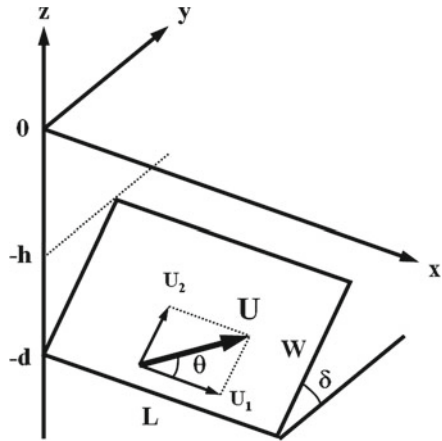
In this section we shall apply the Okada formulae to derive the main regularities relating the parameters of a tsunami source to the respective earthquake magnitude and depth.

In the simplest case the source of a tsunamigenic earthquake can be represented by a rectangular fault with a uniform slip distribution. The Okada formulae presented in the preceding Sect. 2.2 are applicable precisely in the case of such a seismic source. In spite of the Okada formulae being analytical expressions, applying them to reveal general regularities represents a nontrivial problem. The point, here, consists not only in the expressions being cumbersome, but, mainly, in the large number of input parameters. Indeed, the calculation of bottom deformations at the tsunami source with the aid of the Okada formulae requires the following set of input parameters (see Fig. 2.6): the depth d of the fault area, the width W and length L of the fault area, the length of the Burgers vector, $|U|$, the dip angle δ , the angle between the strike direction and the slip direction, θ , the angle between the Burgers vector and the fault plane, γ , and, also, the Lamé coefficients λ and μ , that characterize the elasticity properties of a medium. If calculations are performed for a real event, the above nine parameters must be supplemented with three more quantities: the longitude and latitude of the earthquake epicenter, and, also, the strike angle ϕ . To analyze the general properties of oceanic bottom deformations in a 9-dimensional (11-dimensional) space of input parameters is not only an extremely complicated task, but is also devoid of any practical expediency—it is easier to deal with concrete seismic events, for which all the aforementioned parameters have definite values.

Let us reduce the number of input parameters making use of physically reasonable assumptions and known constraints (Bolshakova and Nosov 2011). We shall, first, assume the Burgers vector to lie in the plane of the fault area: $\mathbf{U} = (U_1, U_2, 0)$ (see Fig. 2.7). Second, we shall consider the Lamé coefficients to be equal to each other, $\lambda = \mu$ (the expediency of this assumption is shown in Sect. 2.2). As additional constraints we shall invoke the definition of the seismic moment (2.1), the relationship between the seismic moment and the moment magnitude (2.2), and, also, the empirical formulae given by Kanamori and Anderson for parameters of the fault area (Kanamori and Anderson 1975):

$$L/W = 2, \quad U/L = 5 \times 10^{-5}. \quad (2.34)$$

Fig. 2.7 Geometry of the source model of an earthquake. L is the length of the fault plane, W is the width of the fault plane, U is the Burgers vector, δ is the dip angle, θ is the rake angle, h is the depth of the upper edge of the fault plane



Formulae (2.1), (2.2) and (2.34) permit to express the dimensions of the fault area and the slip value (the length of the Burgers vector) via the earthquake moment magnitude

$$\log_{10} L[\text{km}] = 0.5 M_w - A_L, \quad (2.35)$$

$$\log_{10} W[\text{km}] = 0.5 M_w - A_W, \quad (2.36)$$

$$\log_{10} U[\text{m}] = 0.5 M_w - A_U. \quad (2.37)$$

The shear modulus entering into formula (2.1) for the seismic moment varies within the range of $3 - 8 \times 10^{10}$ Pa. As a consequence the coefficients involved in formulae (2.35)–(2.37) also undergo insignificant variations: $A_L = 1.92 - 2.07$, $A_W = 2.22 - 2.37$, $A_U = 3.22 - 3.37$. The lower boundaries of the ranges indicated correspond to the minimal value of the shear modulus $\mu = 3 \times 10^{10}$ Pa that is typical for crustal faults. In all further calculations we shall make use of precisely these minimal values ($A_L = 1.92$, $A_W = 2.22$, $A_U = 3.22$)—in this case formulae (2.35)–(2.37) are equivalent to the known expressions presented, for example, in the Handbook for Tsunami Forecast (2001).

Taking into account the adopted assumptions and constraints (2.35)–(2.37), we arrive at a reduced set of input parameters for the Okada formulae, which only includes four quantities: the moment magnitude M_w , the angles Dip (δ), and Rake (θ), as well as the depth d of the earthquake source. In the case of strong shallow earthquakes, which are precisely the most interesting ones as tsunami sources, the source depth and the width W of the fault area are often comparable quantities. If the source depth is set equal to the depth of the lower edge of the fault area and the Dip angle and/or moment magnitude, upon which the width of the fault area depends, are varied, then in a number of cases the fault may emerge at the surface. To prevent the fault from emerging at the surface, it is convenient to consider the source depth

to be equal to the depth of the upper edge of the fault area, $h = d - W \sin \delta$ (see Fig. 2.7). We shall choose precisely this characteristic as a measure of the depth of an earthquake source.

The small number of input parameters permits to apply the Monte Carlo method quite efficiently to reveal general properties of bottom deformations. For example, one of the parameters can be fixed, while variations of the remaining ones are random and statistically uniform within given ranges. Such an analysis was performed by Yoshimitsu Okada in Okada (1995) for a point double-couple source. But these results cannot be applied in analyzing the properties of oceanic bottom deformations in the case of tsunamigenic earthquakes, which, as a rule, are strong and shallow. The source of a tsunamigenic earthquake can evidently not be represented by a point. It is always quite an extended region, the dimensions of which amount to tens and even hundreds of kilometers and in certain cases (for example, Sumatra 2004) exceed a thousand kilometers.

To obtain the relationships between the earthquake parameters and the tsunami characteristics it is additionally necessary to adopt a number of assumptions concerning the mechanism of wave generation. As it was shown in Sect. 2.1, the main effect resulting in the generation of tsunami waves in the case of earthquakes consists in the displacement of water by the residual (coseismic) bottom deformation. Consider a water layer limited by a free surface from above and by the bottom surface of arbitrary form from below. Consider the origin of the reference frame to be situated on the unperturbed water surface. Let the $0z$ axis be directed vertically upward, and the $0x$ and $0y$ axes to the East and North, respectively. Consider the position of the bottom before the earthquake to be determined by the formula

$$z = -H(x, y). \quad (2.38)$$

After the earthquake the bottom occupies a new position:

$$z = -H(x, y) + \eta(x, y), \quad (2.39)$$

where $\eta(x, y)$ is the residual displacement of the bottom surface. To determine the relationship between the vector field of bottom deformations, $\mathbf{D} \equiv (D_x, D_y, D_z)$, and function $\eta(x, y)$ consider a certain point situated on the unperturbed bottom surface, $P_0 = (x_0, y_0, z_0)$. The coordinates of this point satisfy Eq.(2.38). As a result of coseismic deformation after the earthquake the point moves to a new position $P_1 = (x_0 + D_x, y_0 + D_y, z_0 + D_z)$, continuing to remain on the bottom surface. Now, the coordinates of this point satisfy Eq.(2.39) which assumes the following form:

$$z_0 + D_z = -H(x_0 + D_x, y_0 + D_y) + \eta(x_0 + D_x, y_0 + D_y). \quad (2.40)$$

In the practice of numerical tsunami simulation functions, $H(x, y)$ and $\eta(x, y)$, involved in Eq.(2.40), are represented discretely on a certain grid with a spatial increment Δ . This means that the structure of these functions in between the nearest

nodes of the grid remain beyond consideration. It is reasonable to assume that in between nodes functions $H(x, y)$ and $\eta(x, y)$ are sufficiently smooth, for example, linear, otherwise the choice of the grid increment would have to be acknowledged to be erroneous. The grid increment is usually $\Delta \sim 10^3$ m. The coseismic deformation amplitude is significantly inferior to this value: $|\mathbf{D}| \ll \Delta$. Consequently, function $H(x, y)$ in Eq. (2.40) can be expanded into a Taylor series at the point (x_0, y_0) , retaining only linear terms in the expansion. For function $\eta(x, y)$ it is reasonable to adopt an even more simple assumption: $\eta(x_0 + D_x, y_0 + D_y) \approx \eta(x_0, y_0)$. As a result, taking into account Eq. (2.38), we obtain a relationship between the residual displacement of the bottom surface and the vector field of bottom deformations as well as the distribution of depths (Nosov et al. 2014)

$$\eta = \frac{\partial H}{\partial x} D_x + \frac{\partial H}{\partial y} D_y + D_z. \quad (2.41)$$

A similar formula was previously obtained in Tanioka and Satake (1996) on the basis of arguments of a intuitive physical character.

From formula (2.41) it is seen that calculation of the residual displacement of the bottom surface, generally speaking, not only requires information concerning the vector field \mathbf{D} , but also information on the distribution of depths, which is, naturally, individual for each tsunami source. In this connection analysis of the contribution of horizontal components (the first two terms in formula (2.41)) cannot be performed in the general case, i.e., without being related to real tsunami sources. This problem will be dealt with in the next Sect. 2.4. Here, in order to obtain general relationships we shall restrict ourselves to applying the model of an ocean of fixed depth $H = \text{const}$. In this case, only the vertical component of the bottom deformation vector contributes to the generation of tsunami waves: $\eta = D_z$.

Function $\eta(x, y)$, describing displacement of the bottom surface, may exhibit quite a complex structure even in the idealized case of a uniform distribution of the slip along a rectangular fault area (see Fig. 2.8). In the case of real events, with account of bathymetry ($H \neq \text{const}$) and of slip inhomogeneities along the fault surface, the structure of function $\eta(x, y)$, may, evidently, be even more complex.

Which tsunami source parameters, determined by deformation of the bottom, $\eta(x, y)$, should be considered? Generally speaking, quite a significant number of parameters, such as, for example, a set of amplitudes of Fourier harmonics, may be required for a complete description of function $\eta(x, y)$. We must, naturally, not take the path of calculating Fourier harmonics, but will take advantage of a limited number of parameters, each of which has a clear physical meaning and is unambiguously determined by function $\eta(x, y)$. Of all the multitude of such parameters we have found it reasonable to consider the following set of quantities:

1. the double amplitude of vertical bottom deformation:

$$A = \text{Max} [\eta(x, y)] - \text{Min} [\eta(x, y)], \quad (2.42)$$

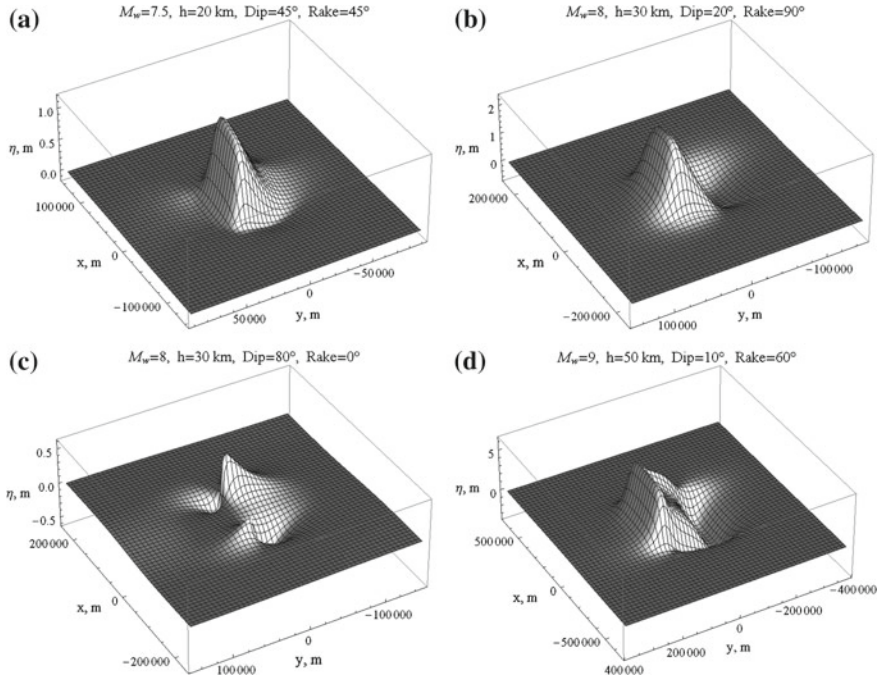


Fig. 2.8 Examples of calculations of the coseismic bottom deformation by the Okada formulae (Okada 1985). The parameters of the rectangular source with uniform distribution of the slip are indicated in figure

2. the absolute value of the displaced water volume:

$$V = \left| \iint \eta(x, y) dx dy \right|, \quad (2.43)$$

3. the potential energy of the initial elevation:

$$E = \frac{\rho g}{2} \iint \eta^2(x, y) dx dy, \quad (2.44)$$

where g is the gravity acceleration, ρ is the density of water (in calculations we assumed $g = 9.8 \text{ m/s}^2$, $\rho = 1000 \text{ kg/m}^3$). In determining energy E we apply the traditional approximation, according to which a bottom deformation immediately gives rise to a perturbation of equivalent shape at the water surface: $\xi = \eta$. The search for extreme values in formula (2.42) and integration in formulae (2.43) and (2.44) was performed over the entire region, where noticeable bottom deformations were observed. In practice this region was defined as follows: $-2L - 2h < x < 3L + 2h$, $-2W - 2h < y < 3W + 2h$. Integration was carried out numerically by the methods of rectangles. The number of rectangular cells in the region amounted to 100×100 .

Let us note a “subtle point” related to calculation of integral (2.43). From the Okada formulae it follows that at large distances from the source the amplitude of the oceanic bottom deformation decreases inversely proportional to the square epicentral distance: $\eta \sim r^{-2}$ (Okada 1995). Consequently, the integral in formula (2.43), if calculated within infinite limits, will diverge. In this connection, the value of the displaced volume, generally speaking, depends on the chosen integration region. However, only significant bottom deformations, occurring in the nearby zone, influence tsunami generation. Calculation of the energy integral (2.44) gives rise to no problems. The drop of the integrand function with distance in formula (2.44) is significantly more rapid ($\eta^2 \sim r^{-4}$), therefore the integral is sure to converge, even in the case of integration within infinite limits.

The amplitude of bottom deformation, A , to a significant extent determines the tsunami runup amplitude—the importance of this characteristic cannot give rise to any doubt. As to the displaced volume V and initial elevation energy E , the significance of these characteristics is confirmed by the fact that in the problem of tsunami propagation in an open ocean both quantities are integrals of motion. Indeed, certain “losses” of displaced volume may occur, but only during the runup process and in the case of sufficiently strong tsunamis, when the waves cover significant distances of land and flood local depressions. Noticeable dissipation of tsunami energy also takes place only in the runup zone (or in shallow water), especially if the propagation of waves is accompanied by their collapse (Li and Raichlen 2002; Bernatskiy and Nosov 2012).

To reveal the dependence of quantities A , V , and E upon the earthquake moment magnitude M_w and depth use was made of the Monte Carlo method. In the first series of calculation variations of the Dip and Rake angles, as well as of the magnitude, were statistically uniform within the following ranges: $0 \leq \delta \leq \pi/2$, $-\pi/2 \leq \theta \leq \pi/2$, $6.5 \leq M_w \leq 9.5$. The depth of the upper edge of the fault area, h , was made to assume fixed values: 0, 10, 30, 100 and 300 km. For each depth value 5000 numerical experiments were performed. The results of calculations, namely the dependencies of quantities A , V and E upon the moment magnitude M_w , are shown in Figs. 2.9, 2.10 and 2.11, respectively.

A common property of the dependences presented consists in that all the parameters investigated tend to exhibit a rapid exponential rise as the earthquake magnitude increases. The dependences are characterized by a significant spread in the data, related to the influence of the orientation of the fault area (the Dip angle) and the slip direction (the Rake angle) on the parameters investigated. The “clouds” of points are characterized by clearly defined upper limits that are determined by the following simple formulae (Bolshakova and Nosov 2011):

$$\log_{10} A_{\max}[m] = 0.5 M_w - 3.22, \quad (2.45)$$

$$\log_{10} V_{\max}[m^3] = 1.5 M_w - 1.8, \quad (2.46)$$

$$\log_{10} E_{\max}[J] = 2.0 M_w - 1.7. \quad (2.47)$$

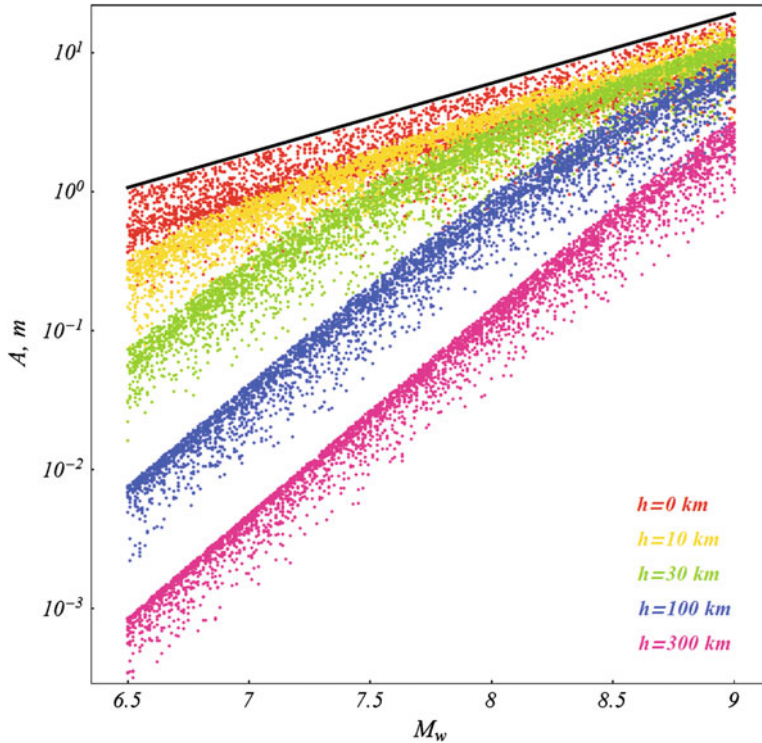


Fig. 2.9 Double amplitude of coseismic bottom deformation at tsunami source versus moment magnitude. The calculation is performed for fixed depth values of the upper edge of the fault area, $h = 0, 10, 30, 100$, and 300 km. Variations of the Dip and Rake angles and, also, of the magnitude were random and statistically uniform within the ranges: $0 \leq \delta \leq \pi/2$, $-\pi/2 \leq \theta \leq \pi/2$, $6.5 \leq M_w \leq 9.5$. The color of the points varies depending on the depth h in accordance with the legend shown in the figure. The black line, marking the upper edge of the “cloud” of points is constructed in accordance with formula (2.45)

The dependences (2.45)–(2.47) are shown by solid lines in the figures. Note that the slip value serves as an upper limit for the amplitude of bottom deformations: the numerical coefficients in formulae (2.37) and (2.45) coincide.

In the case of amplitude A and energy E the dependence upon the earthquake source depth is quite clear. As the depth increases, both quantities decrease noticeably, and the drop is more rapid at smaller magnitudes.

Unlike the amplitude and energy, the displaced volume does not depend on the depth of the earthquake source. This feature can be explained by the drop in the deformation amplitude in the case of a pointlike source (i.e., for each element of the fault area) being inversely proportional to the square distance $\eta \sim r^{-2}$ Okada (1995). Within the area $dx dy$ the elementary volume $dV = \eta dx dy$ is displaced. If one passes to spherical coordinates with the origin at the chosen pointlike source, then $dx dy \sim r^2 d\varphi d\psi$. The quantity dV is seen to be independent of the distance from

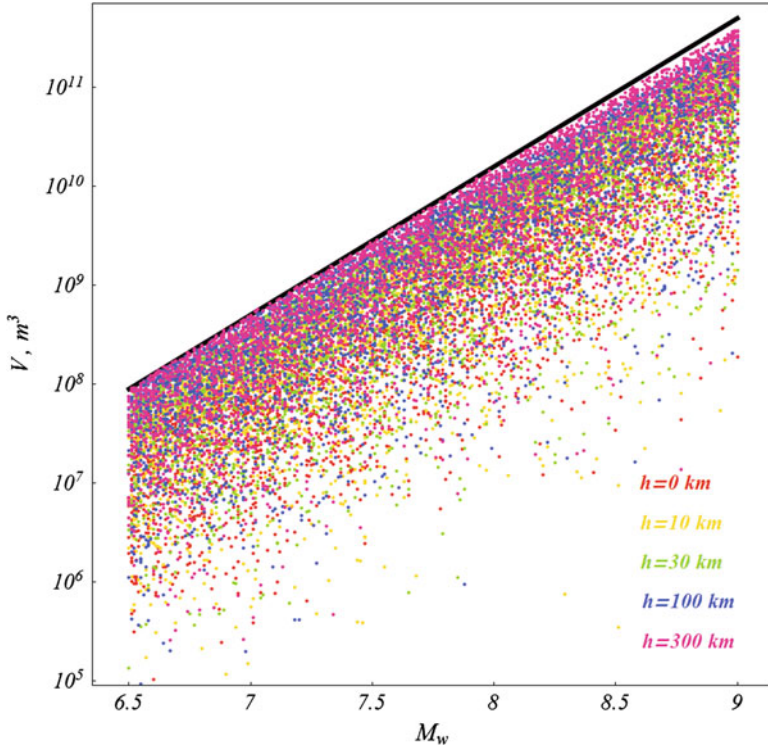


Fig. 2.10 Displaced water volume (its absolute value) at tsunami source versus moment magnitude. The calculation is performed for fixed depth values of the upper edge of the fault area, $h = 0, 10, 30, 100$, and 300 km. Variations of the Dip and Rake angles and, also, of the magnitude were random and statistically uniform within the ranges: $0 \leq \delta \leq \pi/2$, $-\pi/2 \leq \theta \leq \pi/2$, $6.5 \leq M_w \leq 9.5$. The color of the points varies depending on the depth h in accordance with the legend shown in the figure. The black line, marking the upper edge of the “cloud” of points is constructed in accordance with formula (2.46)

the source, r . Consequently, the whole displaced volume should also be independent of the source depth.

By combining formulae (2.45) and (2.46) it is possible to obtain an estimate for the average radius of the tsunami source, ($R_{ts} \equiv \sqrt{V_{\max}/A_{\max}}$):

$$\log_{10} R_{ts}[\text{km}] = 0.5 M_w - 2.29. \quad (2.48)$$

The obtained estimate is in good agreement with the empirical formula (2.5).

From formulae (2.45)–(2.48) it follows that in the case of a magnitude $M_w = 7$ the tsunami source parameters have an upper limit defined by the following values: $A_{\max} = 1.9$ m, $V_{\max} = 5.0 \times 10^8$ m³, $E_{\max} = 2.0 \times 10^{12}$ J, $R_{ts} = 16$ km, while, if $M_w = 9$: $A_{\max} = 19$ m, $V_{\max} = 5.0 \times 10^{11}$ m³, $E_{\max} = 2.0 \times 10^{16}$ J, $R_{ts} = 162$ km.

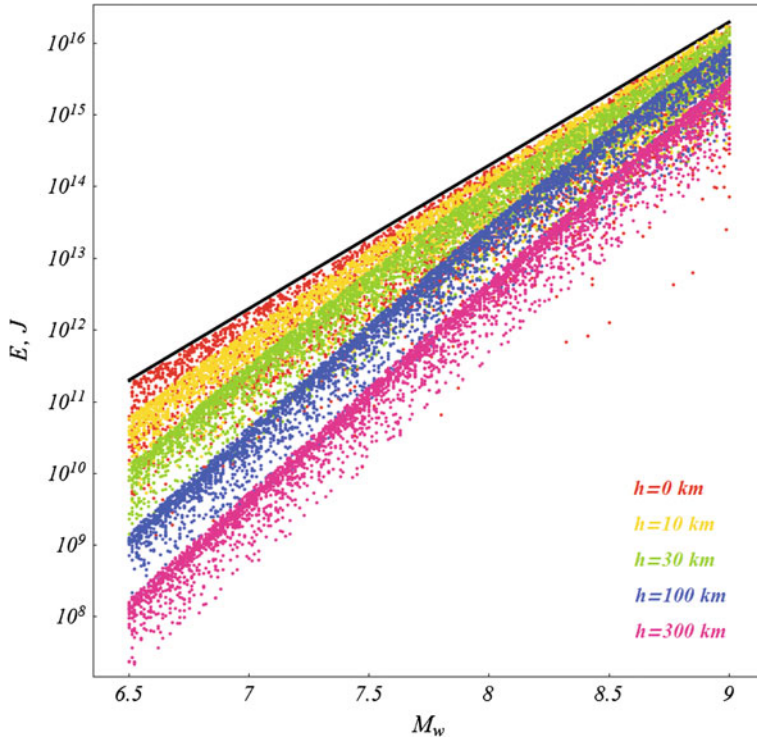


Fig. 2.11 Potential energy of the initial surface elevation at tsunami source versus moment magnitude. The calculation is performed for fixed depth values of the upper edge of the fault area, $h = 0, 10, 30, 100$, and 300 km. Variations of the Dip and Rake angles and, also, of the magnitude were random and statistically uniform within the ranges: $0 \leq \delta \leq \pi/2$, $-\pi/2 \leq \theta \leq \pi/2$, $6.5 \leq M_w \leq 9.5$. The color of the points varies depending on the depth h in accordance with the legend shown in the figure. The black line, marking the upper edge of the “cloud” of points is constructed in accordance with formula (2.47)

Comparison of the tsunami energy determined by formula (2.47) with the known estimate of an earthquake energy (Kanamori 1977)

$$\log_{10} E_{EQ}[J] = 1.5 M_w + 4.8, \quad (2.49)$$

gives an estimate of the part of an earthquake energy contributing to the formation of tsunami waves,

$$\log_{10} E_{\max}/E_{EQ} = 0.5 M_w - 6.5. \quad (2.50)$$

In accordance with formula (2.50) one can conclude that usually quite a small part of the energy of an earthquake is passed on to tsunami waves: between 0.1 % ($M_w = 7$) and 1 % ($M_w = 9$). Hence follows an important world-outlook conclusion. From the point of view of energy, tsunami waves, that carry an enormous destructive potential, only represent a weak “echo” of a catastrophic earthquake.

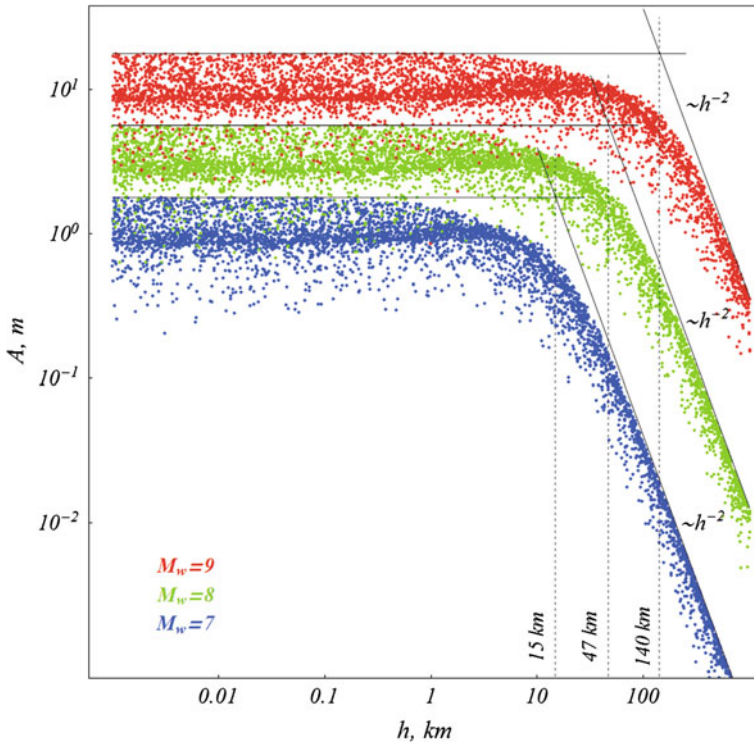


Fig. 2.12 Double amplitude of coseismic bottom deformation at tsunami source versus depth of earthquake. The calculation was performed for fixed values of the moment magnitude $M_w = 7, 8$, and 9 . Variations of the Dip and Rake angles and, also, of the quantity $\log_{10} h$ were random and statistically uniform within the ranges: $0 \leq \delta \leq \pi/2$, $-\pi/2 \leq \theta \leq \pi/2$, $0 < \log_{10} h[m] < 5.8$. The color of the points varies depending on the magnitude M_w in accordance with the legend shown in the figure

The aim of the second series of Monte Carlo calculations was to reveal the character of the dependence of the amplitude A and energy E on the earthquake depth. Three fixed values were chosen for the magnitude: $M_w = 7, 8, 9$. The angles Dip and Rake, as well as the quantity $\log_{10} h$, underwent variations that were statistically uniform within the following ranges: $0 \leq \delta \leq \pi/2$, $-\pi/2 \leq \theta \leq \pi/2$, $0 < \log_{10} h[m] < 5.8$ ($1 \text{ m} < h < 700 \text{ km}$). For each value of the magnitude 5000 numerical experiments were performed. The results of calculations are shown in Figs. 2.12 and 2.13.

From Figs. 2.12 and 2.13 it is seen that in spite of a significant spread in the data a general tendency can be clearly traced: the amplitude and energy are independent of the earthquake source depth up to certain critical values of the quantity h . In the case of large depths both quantities undergo a decrease that is inversely proportional to the square source depth: $A \sim h^{-2}$, $E \sim h^{-2}$. The first regularity follows directly from the law, according to which the deformation amplitude decreases with distance: $\eta \sim r^{-2}$ (Okada 1995). To obtain the second regularity it is necessary to take into

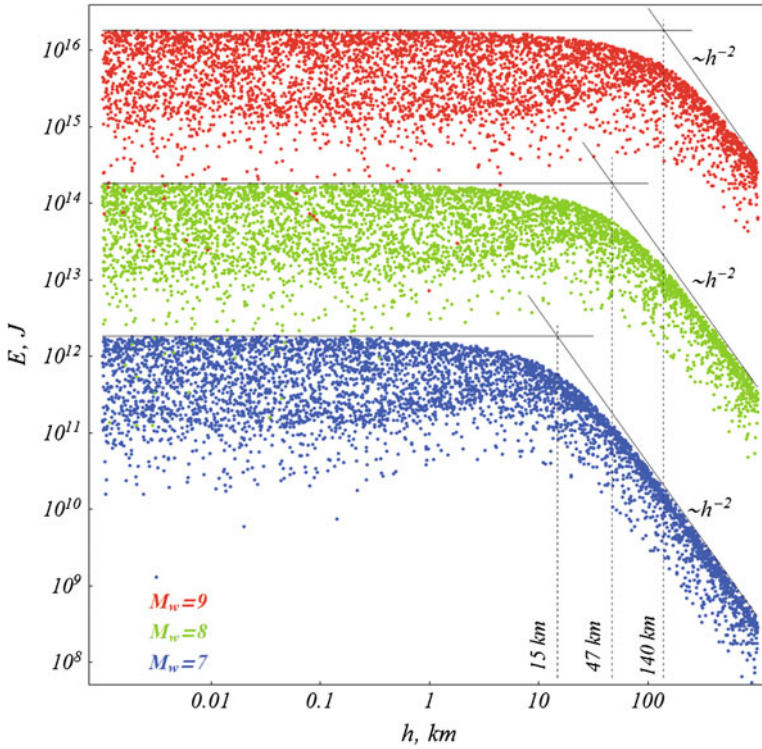


Fig. 2.13 Potential energy of the initial surface elevation at tsunami source versus earthquake depth. The calculation was performed for fixed values of the moment magnitude $M_w = 7, 8$ and 9 . Variations of the Dip and Rake angles and, also, of the quantity $\log_{10} h$ were random and statistically uniform within the ranges: $0 \leq \delta \leq \pi/2$, $-\pi/2 \leq \theta \leq \pi/2$, $0 < \log_{10} h[m] < 5.8$. The color of the points varies depending on the magnitude M_w in accordance with the legend shown in the figure

account that the area encompassing noticeable deformations increases with the source depth: $S \sim h^2$. Therefore, the energy, that is proportional to the product of the square deformation times area, decreases according to the indicated law: $E \sim \eta^2 S \sim h^{-2}$.

From Figs. 2.12 and 2.13 it is possible for each magnitude to determine the critical source depth h_c , beyond which the amplitude and energy start to decrease sharply with the depth. Let us describe the scheme for determining critical values of h_c . At small depths a horizontal straight line is constructed along the upper edge of the “cloud” of points, at large depths a straight line corresponding to the h^{-2} law is constructed. The intersection point of the straight lines determines the sought value of h_c . The critical depth h_c increases with the moment magnitude. It is remarkable that the values of h_c , determined from the dependences for the amplitude and for the energy, are practically equivalent. The critical depths have the following values: $h_c^{M_w 7} \approx 15 \text{ km}$, $h_c^{M_w 8} \approx 47 \text{ km}$, $h_c^{M_w 9} \approx 140 \text{ km}$. The weakening influence of the earthquake source depth starts to manifest itself precisely at these critical values.

To conclude this section we wish to warn against direct application of the theoretical regularities obtained herein in practice, for example, in tsunami warning systems. Real tsunamigenic earthquakes are significantly more complex objects than the model rectangular seismic source dealt with here. The properties of realistic tsunami sources, the coseismic bottom deformations at which are reconstructed with account of the slip structure at the earthquake source, will be analyzed in the following section.

2.4 Properties of Coseismic Deformations of the Oceanic Bottom According to Data on the Slip Structure at Tsunamigenic Earthquake Sources

Publications dedicated to reconstruction of the structure of an earthquake source from the seismic wave field first appeared in the 70s–80s of the twentieth century (Alewine and Jordan 1973, Jovanovich 1975, Pavlov and Gusev 1980, Ward and Barrientos 1986). The significant progress achieved in recent years has provided the possibility of obtaining unique information, namely realistic estimates of slip distributions at earthquake sources (Bassin et al. 2000, Ji et al. 2002, Lay et al. 2011, Shao et al. 2011, Yagi and Fukahata 2011). At present, not only “teleseismic data” are applied in reconstruction of coseismic slip distributions. Here, methods for the inversion of “geodetic data” (e.g., Ozawa et al. 2011, Pollitz et al. 2011), of “strong motion data” (e.g., Kurahashi and Irikura 2011, Suzuki et al. 2011), of “tsunami data” (e.g., Satake 1987, Fujii et al. 2011), and, also, for the “joint inversion of multiple data sets” (e.g., Koketsu et al. 2011, Wei et al. 2012) have proved to be quite opportune.

For reasons of brevity we shall further simply call coseismic slip distributions “slip distributions” or FFM (Finite Fault Model) distributions.

In the case of underwater earthquakes data on slip distributions are particularly valuable: they permit to reconstruct coseismic ocean bottom deformations at the tsunami source, which, in turn, provides the possibility of describing tsunami wave generation. That such a method of reconstructing bottom deformations is adequate is confirmed by the decent agreement between calculated and measured (using the deep-water stations DART, JAMSTEC, and others) waveforms (Laverov et al. 2009, Lay et al. 2011, Nosov et al. 2011). It is precisely for this reason that FFM data are widely used by different scientific groups in simulating concrete tsunamis (e.g., Newman et al. 2011, Poisson et al. 2011, Kim et al. 2013, Nosov et al. 2014).

The slip structure at an earthquake source is represented as follows. The fault surface at the source is approximated by one or several plane rectangular fault segments. Each such segment is characterized by its dimensions as well as position and orientation in space (its geographical coordinates, depth, Dip and Strike angles). The segment is divided into a finite number of subfaults of the same size (usually several hundred rectangular subfaults). Set for each subfault are its coordinates (longitude, latitude), depth and Burgers vector, that characterizes the slip extent and direction (as a rule, the length of the Burgers vector and the Rake angle are given). Further-

more, the activation time of each subfault and its rise time are determined—thus is description performed of the fault rupture dynamics.

As an example, Fig. 2.14a presents the slip distribution (the spatial picture) for the tsunamigenic earthquake that took place on November 15, 2006, on the Central Kuril Islands. The source of the data is the site of the US Geological Survey (Ji 2006). In this particular case, the fault surface is represented by a single segment of dimensions 400 km (along the strike) by 137.5 km. The segment is divided into 220 subfaults (20 km by 12.5 Km each). The maximum slip was 8.9 m.

Figure 2.14b demonstrates the example of a slip distribution, when the fault surface is represented by six fault segments. In this case the data used were obtained in Rhie et al. (2007) the 2004 Sumatra–Andaman earthquake. The total number of subfaults amounted to 201 (66 + 55 + 20 + 20 + 20 + 20). The dimensions of the subfaults were approximately 30 × 30 km (the size of a subfault varied insignificantly from one segment to another). The maximum slip related to the southern fault segment amounted to 35.32 m.

The vector field of coseismic deformation \mathbf{D} can be calculated by the slip distribution, for example, applying the Okada formulae (see Sect. 2.2). The contribution of each subfault to the deformation is calculated independently. The resulting deformation is obtained by summing up the contributions from all the elements (subfaults).

In Fig. 2.15, examples are presented of the calculation of coseismic ocean bottom deformations based on the slip distribution data shown in Fig. 2.14. The black dotted line shows the projection of fault segments onto the surface of the oceanic bottom. The vertical deformation component D_z is shown by isolines (uplifts by red lines, subsidences by blue lines). The green arrows indicate the horizontal deformation component $D_{xy} \equiv (D_x, D_y)$. The maximum uplift and subsidence values, as well as the horizontal deformation amplitude, are indicated in the lower parts of the figures.

Attempts to study the general properties of bottom deformations at tsunami sources, reconstructed from slip distribution data, were first made in Bolshakova and Nosov (2011), Nosov et al. (2014). These works were based on a relatively small set of data presented on the sites of the California Institute of Technology (Caltech), the University of California, Santa Barbara (UCSB), and the US Geological Survey (USGS). Recently, access became open to the database SRCMOD (Finite-Source Rupture Model Database, <http://equake-rc.info/SRCMOD/>), which integrates practically all presently available information on FFM. In this section we shall analyze the general properties of residual bottom deformations at underwater earthquake sources on the basis of a largest possible sample from the database SRCMOD: 200 source models (slip distributions), constructed by different scientific groups for 75 earthquakes during the period between 1923 and 2013 (Bolshakova et al. 2015). In the statistical analysis presented below we shall consider each such source model as an independent realization.

The vector field of oceanic bottom deformations was calculated from slip distributions for each one of the 200 models using the Okada formulae. Then, with the use of formula (2.41) the functions describing displacement of the bottom surface were reconstructed. In calculations, the GEBCO-08 bathymetry with a resolution of 30 ang. sec. was used.

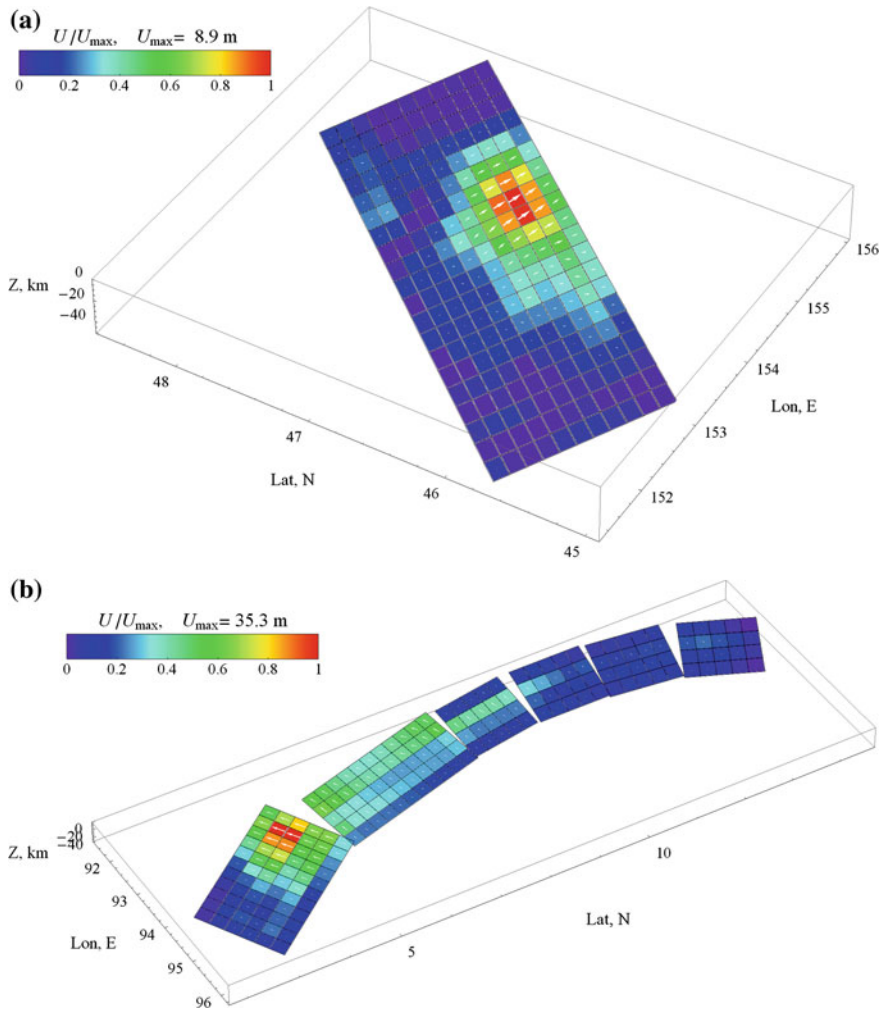


Fig. 2.14 Slip distributions at the 2006 earthquake source on the Central Kuril Islands (a) and at the 2004 Sumatra-Andaman earthquake source (b), based on the data of Ji (2006) and Rhie et al. (2007), respectively. The colors show the amplitudes of dislocations and the white arrows represent the motion of the hanging wall relative to the footwall. The color scale and the maximum slip (dislocation) are presented in the figures

We shall consider the following as the parameters of a tsunami source: the double amplitude of the vertical bottom deformation, A , the displaced water volume V and the initial elevation potential energy E . The quantities indicated are determined by formulae (2.42)–(2.44) in Sect. 2.3. Calculation of the maximum and minimum values, as well as integration in formulae (2.42)–(2.44) was performed over the entire region, where bottom deformations had noticeable values. For coastal sources the land region was not taken into account in calculations. We note that in calculat-

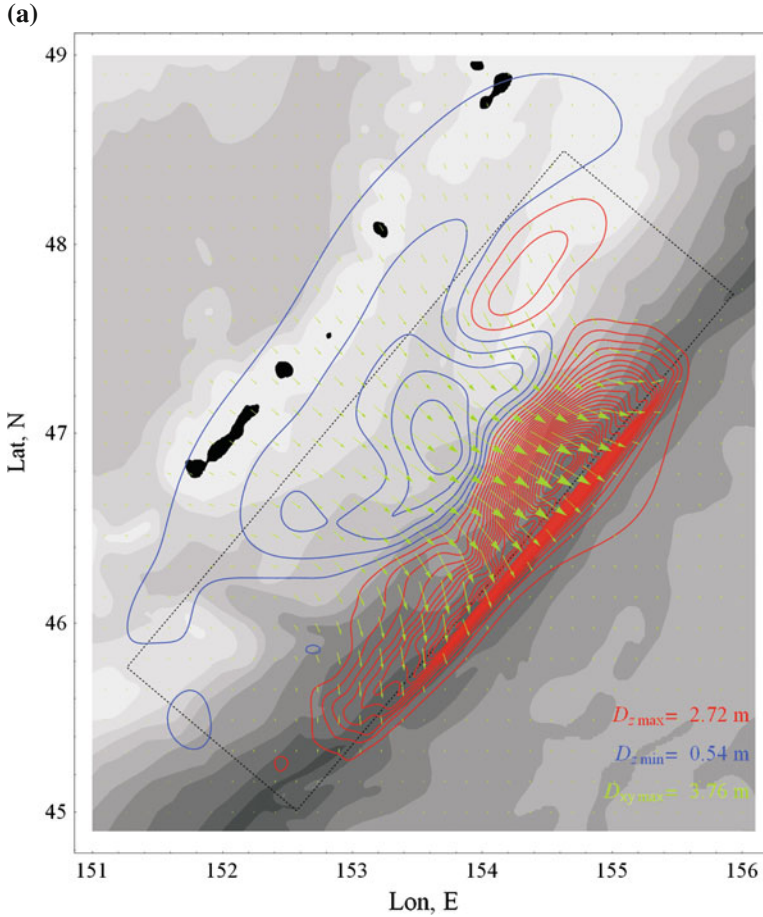


Fig. 2.15 Bottom topography and vector fields of coseismic ocean bottom deformation for the 2006 earthquake on the Central Kuril Islands (a) and the 2004 Sumatra–Andaman earthquake (b). The isobaths are drawn with an interval of 1 km. The vertical bottom deformation is shown by isolines (uplifts in red, subsidences in blue) drawn in steps of 0.1 m (a) and 0.5 m (b). The green arrows stand for the horizontal bottom deformation. The dashed rectangles represent projections of the fault segments onto the surface of the ocean bottom. The maximum uplift and subsidence values, as well as the horizontal deformation amplitudes, are shown in the lower parts of the figures

ing energy we conventionally assume the initial elevation ξ to be equivalent to the coseismic displacement of the bottom surface, η : $\xi = \eta$. Strictly speaking, owing to a “smoothing effect” functions ξ and η may differ from each other (e.g., Kajiura 1963, Nosov and Kolesov 2009, 2011). Neglecting the “smoothing effect” leads to a certain overestimation of the energy. This effect will be dealt with in detail in Sect. 3.5.

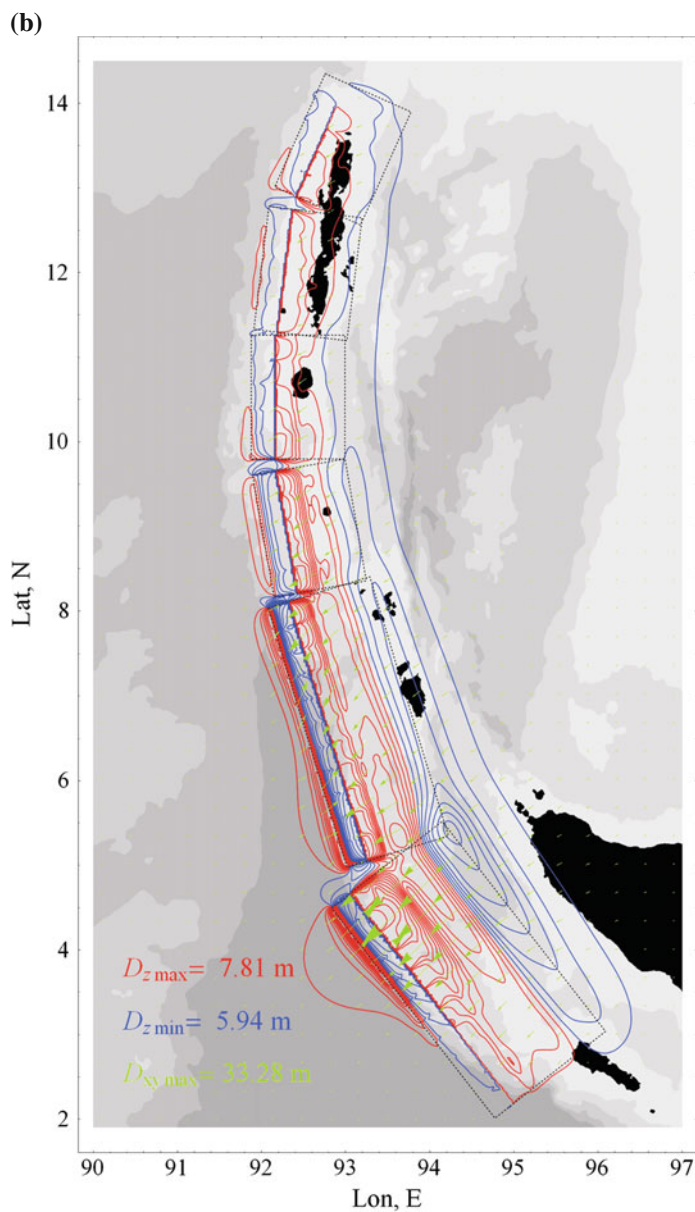


Fig. 2.15 (continued)

Figure 2.16 presents the bottom deformation amplitude versus the moment magnitude of earthquake. The dependence is characterized by quite a significant spread in the data: the correlation coefficient amounts to 0.8. The spread in the data is due to the bottom deformation being sensitive not only to the magnitude, but, also, to the

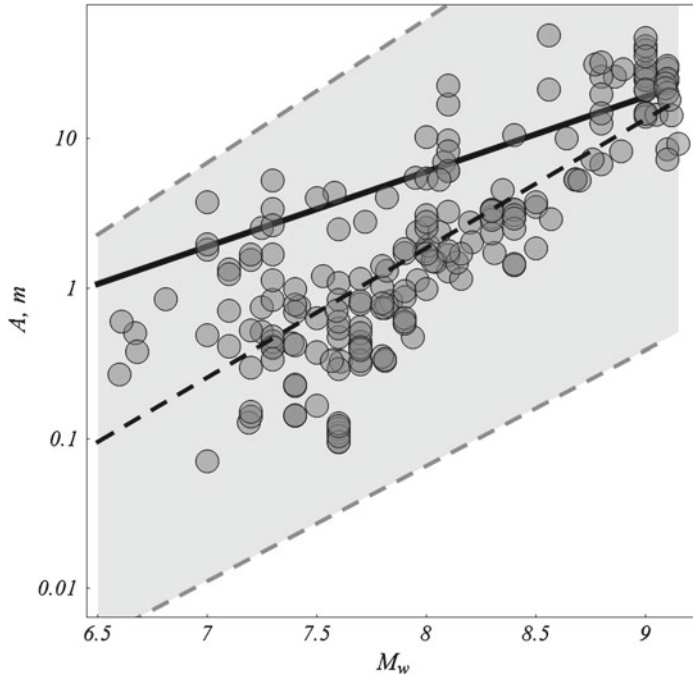


Fig. 2.16 Amplitude of bottom deformation versus earthquake moment magnitude: points—calculation based on data on slip distribution, *dotted line*—regression dependence, *gray band*—95 % confidence interval, *solid line*—theoretical maximum calculated by formula (2.45)

fault area orientation, to the slip direction and distribution, to the earthquake depth. The double amplitude is seen from the figure to vary between several centimeters (7 cm) and several tens of meters (48.5 m) and on the average to rapidly increase exponentially with the magnitude. The regression dependence, constructed by the least-squares method exhibits the following form:

$$\log_{10} A[m] = (0.86 \pm 0.09) M_w - (6.61 \pm 0.73), \quad (2.51)$$

The interval estimates correspond to 95 % probability. The regression dependence (2.51) is shown in Fig. 2.16 by the black dotted line. The gray band within gray dotted lines corresponds to the confidence interval. The solid black line in Fig. 2.16 is the theoretical dependence for the maximum possible deformation amplitude that was obtained in the previous section for the model of a uniform slip along a rectangular fault area (see formula (2.45) from Sect. 2.3). It can be seen that for a significant part of real events, and especially in the case of events with large magnitudes, the bottom deformation amplitude can exceed the theoretically maximum value. This fact is not a paradox. It is due to slip concentration within a narrow region of the fault area.

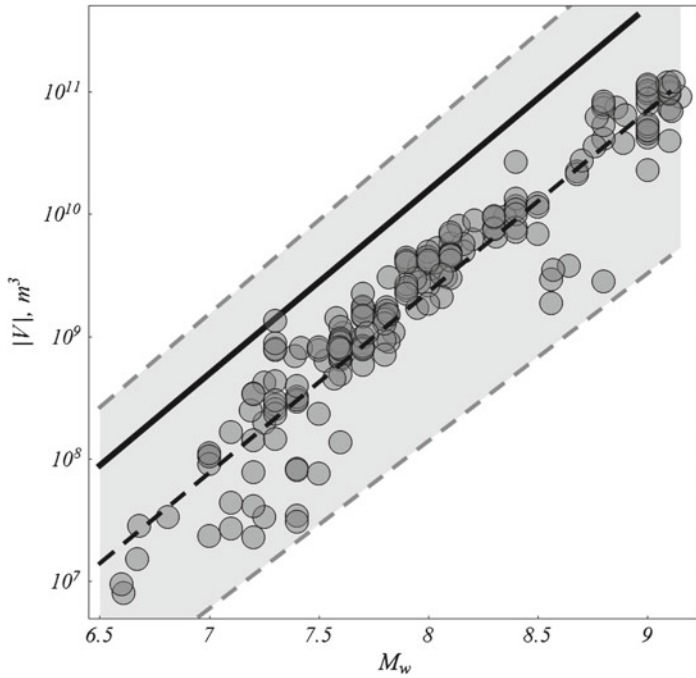


Fig. 2.17 Absolute value of water volume displaced by residual bottom deformation versus earthquake moment magnitude: points—calculation based on data on slip distribution, *dotted line*—regression dependence, *gray band*—95 % confidence interval, *solid line*—theoretical maximum calculated by formula (2.46)

The uniform slip distribution along the whole fault area, the seismic moment (and the moment magnitude) being conserved, would evidently lead to a decrease in the bottom deformation amplitude.

The relationship between the absolute value of the entire displaced volume and the moment magnitude is presented in Fig. 2.17. The displaced volume varies between 0.08 and 121 km³ and on the average exhibits a rapid exponential rise as the moment magnitude increases. As compared to the bottom deformation amplitude the displaced volume is noticeably better correlated with the moment magnitude: the correlation coefficient amounts to 0.95. The respective regression dependence, constructed by the least-squares method, has the following form:

$$\log_{10} V [m^3] = (1.48 \pm 0.09) M_w - (2.45 \pm 0.89), \quad (2.52)$$

The dependence (2.52) is shown in Fig. 2.17 by the black dotted line. The gray band within gray dotted lines corresponds to a 95 % confidence interval.

The solid black line in Fig. 2.17 represents the theoretical dependence for the maximum possible value of the displaced volume, that was obtained within the framework

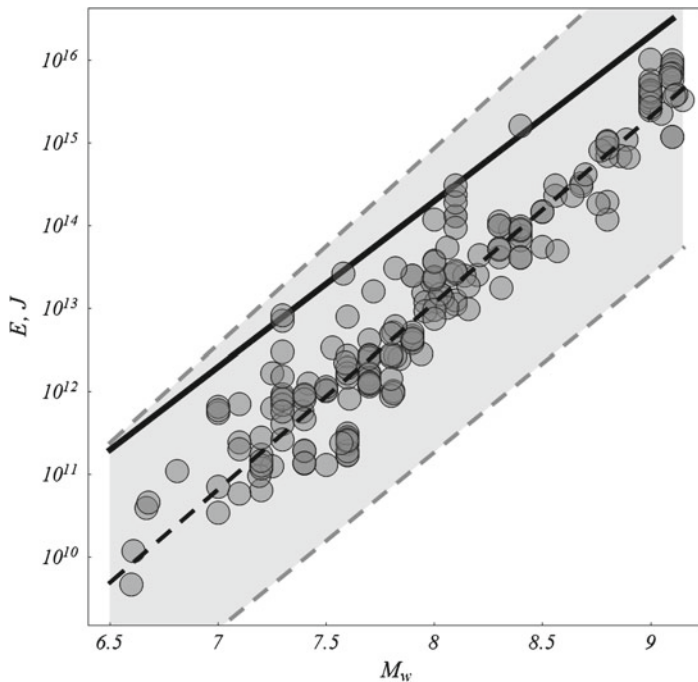


Fig. 2.18 Potential energy of water surface elevation equivalent in shape to residual bottom deformation (the tsunami energy) versus the earthquake moment magnitude: points—calculation based on data on slip distribution, *dotted line*—regression dependence, *gray band*—95 % confidence interval, *solid line*—theoretical maximum calculated by formula (2.47)

of the uniform slip distribution model (see formula (2.46) from Sect. 2.3). The displaced volume, calculated for real events, is seen to never exceed the theoretical maximum value, and, on the average, it usually turns out to be several times smaller than this value.

The dependence of the initial elevation potential energy E upon the moment magnitude is presented in Fig. 2.18. In the case of real events the energy estimate varies within the range from 4.62×10^9 up to 1.01×10^{16} J. On the average, the energy increases exponentially with the moment magnitude. The dependence is characterized by quite a high correlation coefficient—0.94. The regression dependence has the following form:

$$\log_{10} E[J] = (2.26 \pm 0.13) M_w - (4.93 \pm 0.92). \quad (2.53)$$

Dependence (2.53) is shown in the figure by the black dotted line. The gray band within dotted lines corresponds to a 95 % confidence interval. It is seen that, like in the case of the displaced volume, the potential energy calculated for real sources never exceeds the maximum theoretical value (see formula (2.47) from Sect. 2.3).

Applying the regression dependence for the energy of the initial elevation, (2.53), and the Kanamori formula (2.49) for the energy of an earthquake, we obtain the improved (as compared to formula (2.50) from Sect. 2.3) estimate of the part of the earthquake energy that is transmitted to tsunami waves,

$$\log_{10} E/E_{EQ} = 0.75M_w - 9.73. \quad (2.54)$$

From formula (2.54) it follows that the part of energy transmitted to the tsunami increases with the magnitude from 0.003 % (when $M_w = 7$) up to 0.1 % (if $M_w = 9$). On the whole, from the analysis of realistic oceanic bottom deformations at a tsunami source it follows that the part of energy transmitted to tsunami waves turns out to be noticeably smaller than what follows from their theoretical estimates (2.50), presented in Sect. 2.3.

To conclude this section we shall deal with revelation of the role of horizontal deformation components of an uneven (inclined) oceanic bottom in the case of tsunami wave generation. We note that analysis of the double amplitude A is of no particular interest in this case. This is so because the quantity A is actually determined by the values of function η at only two points, at which function η assumes its maximum and minimum values. The components of function η , that are due to the horizontal and vertical components of the bottom deformation, are characterized by nearly a total absence of correlation and by significant variability. Contrary to the versatile “point” quantity A , integral characteristics, such as the displaced volume V and the initial elevation energy E , evidently exhibit greater stability, which permits, on their basis, to introduce quantitative characteristics describing the contribution to tsunami waves of horizontal deformation components in the case of an uneven bottom.

The structure of formula (2.41) itself immediately permits to unambiguously determine the contribution of horizontal deformations of an inclined bottom to the total displaced volume:

$$V_{xy} = \iint \left(\frac{\partial H}{\partial x} D_x + \frac{\partial H}{\partial y} D_y \right) dx dy. \quad (2.55)$$

We determine the contribution of horizontal deformations to the initial elevation potential energy as follows:

$$E_{xy} = E - E_z, \quad (2.56)$$

$$E_z = \frac{\rho g}{2} \iint (D_z)^2 dx dy, \quad (2.57)$$

where E is the potential energy calculated with account of all the bottom deformation components by formula (2.44).

Figure 2.19 illustrates the contribution of horizontal deformations of an inclined bottom, V_{xy} , to the total displaced volume V . Both quantities can be either positive or negative. For clarity we present linear equivalents of the volumes retaining their

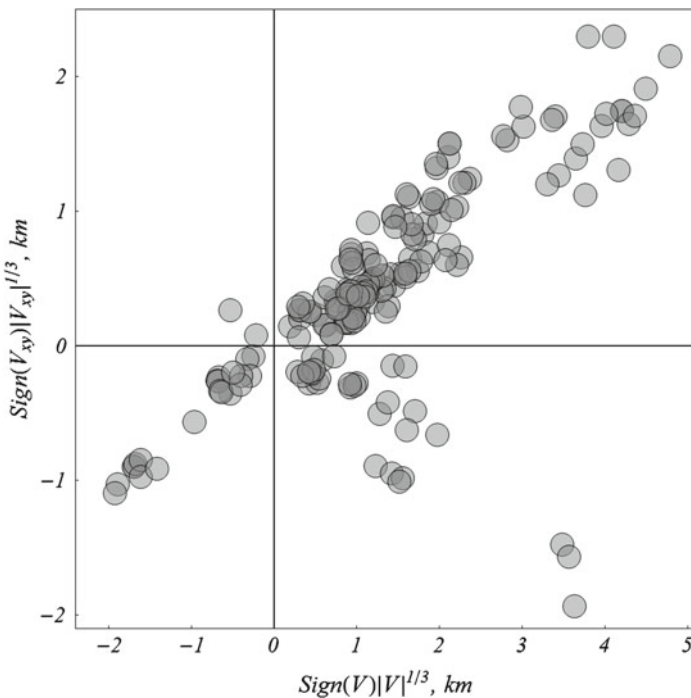


Fig. 2.19 Volume of water displaced by horizontal deformation components of inclined bottom, V_{xy} , versus total displaced volume V . The axes represent linear equivalents of the displaced volumes with their signs retained

signs: $Sign(V) |V|^{1/3}$ and $Sign(V_{xy}) |V_{xy}|^{1/3}$. From the figure it is seen that in most cases (163 out of 200) the signs of quantities V_{xy} and V coincide. This impressive result signifies that, as a rule, horizontal bottom deformations provide an additional contribution to the displaced volume. This result was first obtained in Nosov et al. (2014). In absolute value, the contribution of horizontal bottom deformation components to the displaced volume V_{xy}/V varies between 0.1 and 88%, while its mean value amount to 15%. Hence follows an important, from a practical point of view, conclusion: neglecting the horizontal bottom deformation components in simulating a tsunami in most cases leads to noticeable, while sometimes to significant, underestimation of the wave.

Figure 2.20 presents the part of potential energy of the water surface elevation, that is due to the contribution of horizontal deformation components of an inclined bottom, E_{xy}/E , versus the total potential energy E . The value of E_{xy}/E can be either positive or negative ($-0.08 < E_{xy}/E < 0.41$). In most cases (173 out of 200) the contribution of horizontal deformation is positive. In other words, horizontal components of the bottom deformation, as a rule, give an additional contribution to the tsunami energy. It is remarkable that not only for the displaced volume, but for the tsunami energy, also, this contribution is not negligible.

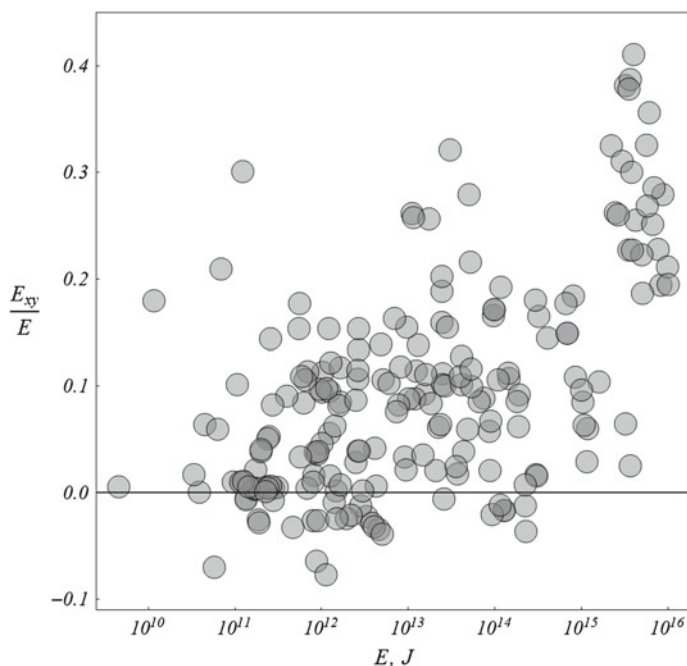


Fig. 2.20 Relative contribution of horizontal bottom deformation components to tsunami energy versus total energy value

The fact that in most cases horizontal deformations of an inclined bottom provide an additional contribution both to the volume of water displaced at the source and to the tsunami energy points to the existence of a certain correlation between the ocean bottom relief and coseismic deformations. To explain the existence of such a correlation it suffices to recall that most tsunamigenic earthquakes are related to subduction zones (e.g., Satake and Tanioka 1999, Gusiakov 2014), which are characterized by certain inherent shapes of the oceanic bottom, such as, for example, deep-water trenches. And, although each seismic event is individual, the occurrence of earthquakes in subduction zones is on the whole consistent with certain “scenarios”, a manifestation of which consists precisely in the observed correlation between vertical and horizontal coseismic shifts of underwater slopes.

2.5 Distribution of Tsunami Sources in Space and Time

The problem of studying the origination periodicity of tsunami sources in space and time continues to be one of the hitherto unresolved fundamental scientific problems, and it is also very important from the point of view of applications (Mogi 1979, Kasahara 1981, Riguzzi et al. 2010, Levin and Sasorova 2012). Sources of tsunami-

genic earthquakes cannot arise at any point whatever of the World Ocean. Thus, for example, practically no tsunami sources have ever existed within regions between latitudes 70 and 90 North as well as between latitudes 40 and 90 South. In other words, from the point of view of the origination of seismotectonic tsunamis high latitudes are sort of forbidden zones. Still another natural event must be noted: at low latitudes, where the occurrence of tsunami sources is quite customary, there also exists a clearly identifiable forbidden zone between latitudes 20 and 30 North. No tsunamis were observed to arise within this band during the past 100 years. Why? Of course, we cannot provide an answer to this question in the present section, and we will only present a number of observed facts, that in the future may facilitate comprehension of the physics of the Earth's seismicity and, in particular, explanation of the existing space–time regularities characteristic of the distribution of tsunami sources.

Analysis of the space–time distributions of tsunamigenic earthquake sources was performed taking advantage of the material provided by two known tsunami databases, NOAA/WDS Global Historical Tsunami Database at NGDC (http://www.ngdc.noaa.gov/hazard/tsu_db.shtml) and Historical Tsunami Database for the World Ocean (<http://tsun.sccc.ru/tsunami-database/index.php>).

The aforementioned databases were used to form an operational catalogue for the period from 1900 up to 2012 containing events involving tsunamigenic earthquakes (EQ) of magnitude $M \geq 7.5$, intensity $I \geq 1.0$, and validity $V = 4$ (i.e., only authentically registered events). After the elimination of duplicates, a cross-check and correction of both databases 99 events were ultimately singled out and identified as tsunamis of tectonic origin.

The statistical peculiarities of tsunamigenic events revealed with account of geographical and magnitude parameters of the distributions permit to answer the following question: what fraction of strong EQ happens to be tsunamigenic EQ when a change occurs in the threshold value of the magnitude.

In Table 2.2 the numbers of events over all the Earth and, separately, the individual hemispheres are presented for the following variations in the magnitude threshold: $M \geq 7.5$; $M \geq 8.0$; $M \geq 8.5$. On the average, tsunamigenic earthquakes are seen to compose 16 % (of the entire number of strong EQ, equal to 615), and in the case of events with $M \geq 7.5$ and events with $M \geq 8.0$ the relative amount of events in the Southern hemisphere is greater than in the Northern hemisphere for both bands of magnitudes. This means that the relative number of tsunamigenic earthquakes does not increase with the magnitude.

However, all catastrophic events (with $M \geq 8.5$) are tsunamigenic. The sources of these events are situated in the region of the Pacific Ocean (4 in South America, 3 in the northern part of the subequatorial region, 1 in the Kamchatka region, 1 in Japan). We note that the above features of the distribution of tsunamigenic earthquakes were dealt with in a series of publications (Levin 2006, Levin and Sasorova 2010, Levin and Sasorova 2014).

Table 2.2 Comparison of the number of strong earthquakes (EQ) with the number of tsunamigenic earthquakes (TEQ) of the same magnitude

	The whole Earth	Northern hemisphere	Southern hemisphere
Events with $M \geq 7.5$			
Total number of EQ	615	390	225
Number of TEQ, with $I \geq 1$	99 (16 %)	51 (13 %)	48 (21 %)
Events with $M \geq 8.0$			
Total number of EQ	292	192	100
Number of TEQ, with $I \geq 1$	47 (16 %)	28 (15 %)	19 (19 %)
Events with $M \geq 8.5$			
Total number of EQ	9	5	4
Number of TEQ, with $I \geq 1$	9 (100 %)	5 (100 %)	4 (100 %)

Construction of the spatial distributions of tectonic tsunami sources was based on division of the Earth's surface into 18 latitudinal bands, the size of each latitudinal band being 10° . Separation was also performed of events that occurred in the Northern and Southern hemispheres of the Earth. In analyzing time distributions the entire interval of observation was divided into 5-year intervals, and the total number of events as well as the total energy released was considered for each 5-year interval.

Since most seismic events occur near the boundaries of lithospheric plates, use was made in the work of the event density and of the energy density (the number of earthquakes and the energy released normalized to the boundary length of the lithospheric plates in each latitudinal band). Such normalization yields the “power” of the given segment of a plate boundary: the mean number of earthquakes or the mean energy value per each 100 kilometers of plate boundary. Utilization of these characteristics, that have a clear physical meaning, permits to compare the seismic activities of latitudinal bands and of different parts of the terrestrial globe (Levin and Sasorova 2012).

Figure 2.21 shows the latitudinal distribution of the number of tsunami sources of tectonic origin. In this distribution one can clearly identify two maxima at latitudes 40° – 50° N and 0° – 10° S, a local minimum in the region of 20° – 30° N and practically zero values at the polar caps and at high latitudes.

Figure 2.21b presents the latitudinal density distribution of the sources of tsunamigenic EQ. The main features of the distribution in Fig. 2.21b are similar to those of the distribution in Fig. 2.21a. However, the maximum in the Northern hemisphere is more sharply outlines, while in the Southern hemisphere the maximum in the region of 0° – 10° S disintegrates into two maxima: at 0° – 10° S and 30° – 40° S. The second maximum is pronounced more weakly.

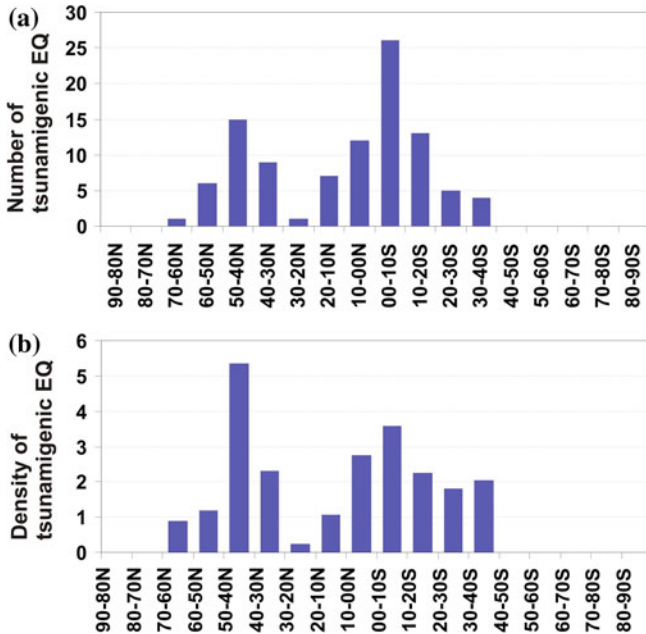


Fig. 2.21 Latitudinal distribution of number of tsunamigenic earthquake sources (a), latitudinal density distribution of tsunamigenic earthquakes (b)

Further, we shall consider latitudinal distributions of the energy released from tsunamigenic EQ (Fig. 2.22a) and of the energy density (Fig. 2.22b). Here, distributions are revealed with three clearly identified local maxima: at 40°–30°N, 10°–00°N and 30°–40°S; in between them there are local minima with practically zero values of energy (and of energy density) at the polar caps and at high latitudes. Of all the energy released from tsunamigenic EQ 22 % is released within the 40°–30°N band of latitudes, 30 % within the 10°–00°N band, and 14 % is released at latitudes of 30°–40°S. All together 66 % of the energy is released at latitudes corresponding to local maxima (three latitudinal bands out of 18).

We shall now present the distribution of events over time. Figure 2.23 shows the source density distributions for tsunamigenic earthquakes over 5-year intervals for the entire Earth (a), for the Northern (b) and Southern (c) hemispheres of the Earth. The scale of the vertical axis remains constant for all three fragments. The periodicity in the increase and decrease of the event density in time is clearly seen. Moreover, an asymmetry is apparent in the increase and decrease of tsunami activity in the Northern and Southern hemispheres. Enhancement of tsunamigenic earthquake activity is displayed alternately in the Northern hemisphere and, then, in the Southern hemisphere (and vice versa).

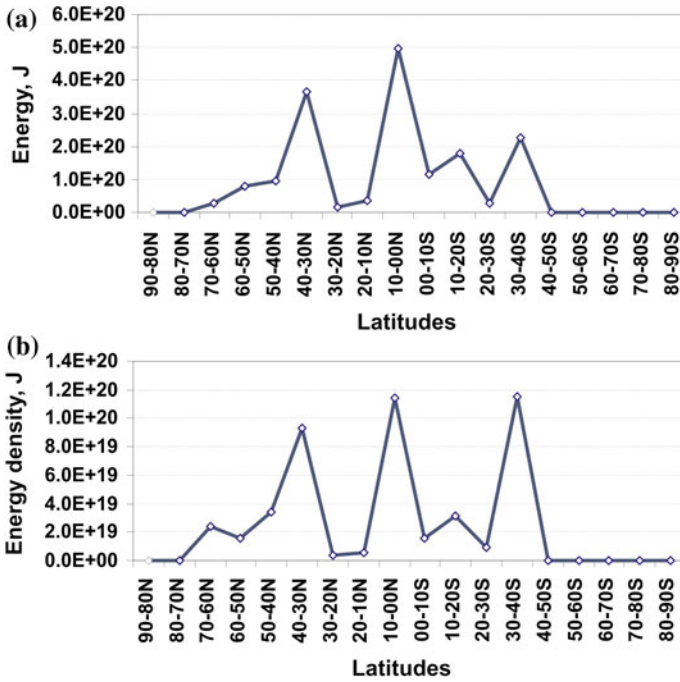


Fig. 2.22 Latitudinal distribution of energy released in tsunamigenic earthquakes (a), latitudinal density distribution of this energy (b)

The most powerful tsunamigenic EQ (from the point of view of the energy release) were observed at the beginning of the twenty-first century. They occurred both in the Northern and Southern hemispheres of the Earth, but within different 5-year intervals. The weakest (in energy) peaks of tsunami activity were at the beginning of the 20 century and at its middle (1950–1965).

Above we dealt separately with latitudinal (spatial) and time distributions of the sources of tectonic tsunamigenic events and with the energy released by these events. However, the most complete picture is provided by two-dimensional (space–time) distributions of events. Such a technique for representing the distributions of seismic activity was first applied in Levin and Sasorova (2010).

The two-dimensional density distribution of tsunamigenic EQ (Fig. 2.24) reveals the existence of regions (polar caps and high latitudes) within which not a single tsunamigenic event occurred during a period more than a hundred years long. The region of high latitudes, where no tsunami sources with $I \geq 1$ were observed, is much more extended in the Southern hemisphere, it starts at 40°S and continues up to the Southern Pole, while in the Northern hemisphere such a region only starts from 70°N. The region with practically zero activity is also found within the latitudinal band of 30°–20°N.

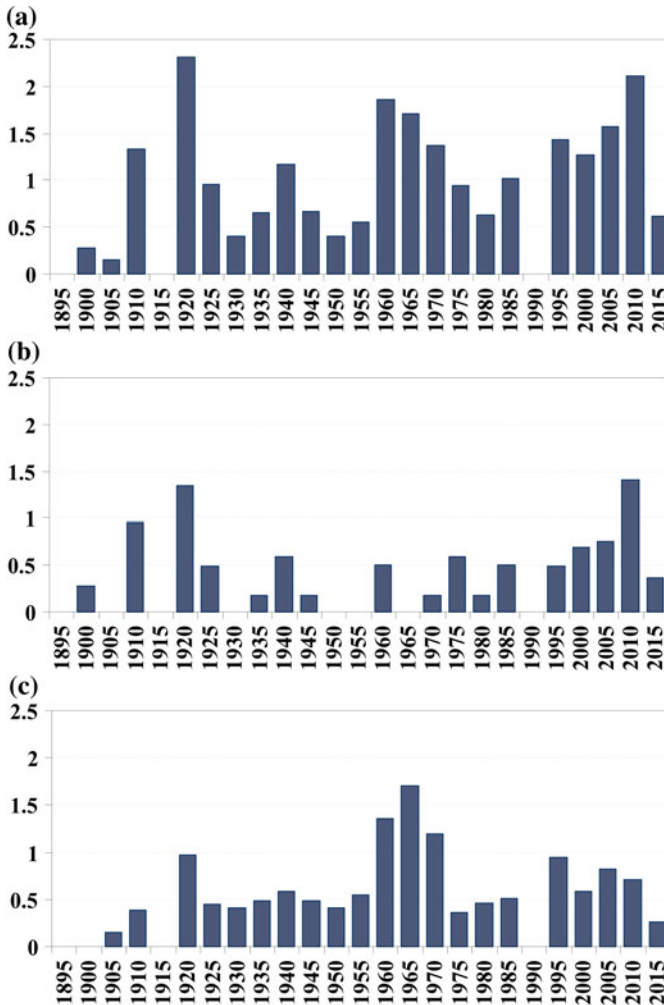


Fig. 2.23 Density distributions of tsunamigenic earthquake sources over 5-year intervals for the entire Earth (a), for the Northern hemisphere (b), for the Southern hemisphere (c)

Periodicity in the origination of tsunamigenic earthquakes is quite pronounced in Fig. 2.24, and this periodicity differs in different latitudinal bands. In the Northern hemisphere powerful peaks of activity were observed, when within a relatively short time interval several significant events took place. Such was the middle of the twentieth century from year 1955 up to 1975, then after a 20-year pause there were events during the period from 1990 up to 2010. Two less powerful clusters were also noted during the period of 1915–1920 and the 1980–1985 time intervals.

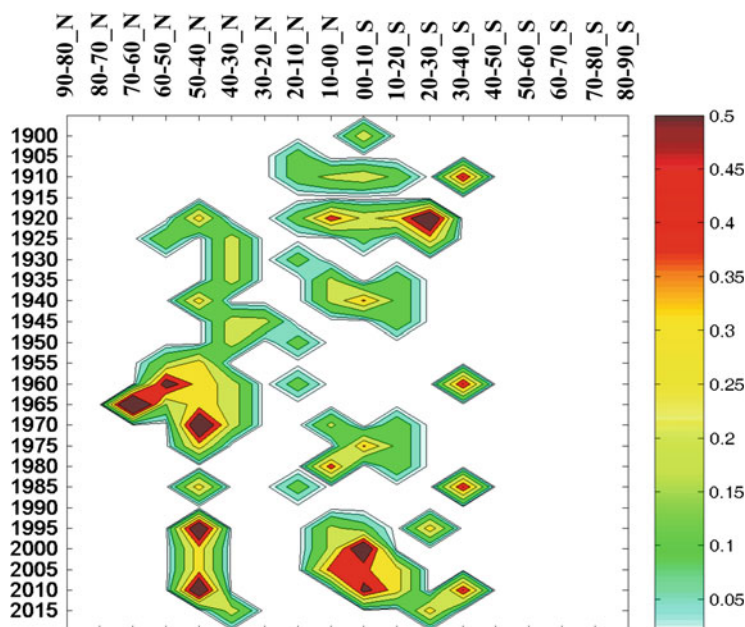


Fig. 2.24 Two-dimensional density distribution of tsunamigenic earthquakes. The *vertical axis* shows time, and the *horizontal axis* shows latitudinal bands. The density of tsunamigenic earthquakes is shown in accordance with the *color scale*

In the subequatorial region peaks of tsunami activity are noted with 25-year intervals (during the first half of the twentieth century), then with 30–40-year intervals (in the middle of the century) and again with an interval of 25 years by the end of the twentieth century. In the Southern hemisphere bursts of tsunami activity, practically identical in power, are noted with a periodicity of 50 years in the first half of the twentieth century, and, then, with a 25-year periodicity between 1960 and present time.

The analysis presented of the distribution of tsunami sources permits to identify the cyclic character of enhancement and attenuation of tsunami activity. Cyclicity is revealed not only in the grouping of events in time, but also in their spatial (latitudinal) grouping. On the one hand, regions are singled out on the surface of the terrestrial globe that exhibit minimal (or zero) tsunami activity—these are regions of high latitudes and Polar Regions. On the other hand, zones are revealed of alternating activity of the process, when adjacent latitudinal zones manifest activity enhancement during different periods of time. High activity in one zone is accompanied by activity attenuation in the adjacent region, and vice versa. Thus, high activity in a certain zone, corresponding to a given time period, is exchanged for a period of relaxation in the neighboring zone.

References

- Alekseev, A.S., Gusiakov, V.K.: Numerical modeling of tsunami and seismic surface wave generation by a submarine earthquake. In: Heath, R.A., Creswell, M.M. (eds.) *Proceedings of Tsunami Res. Symposium*, pp. 243–252. Roy. Soc. New Zealand, Wellington (1976)
- Alewine, R.W., Jordan, T.H.: Generalized inversion of earthquake static displacement fields. *Geophys. J. R. Astron. Soc.* **35**, 357–380 (1973)
- Bassin, C., Laske, G., Masters, G.: The current limits of resolution for surface wave tomography in North America, EOS. *Trans. Am. Geophys. Un.* **81**, F897 (2000)
- Bernatskiy, A.V., Nosov, M.A.: The role of bottom friction in models of nonbreaking tsunami wave runup on the shore. *Izv. Atmos. Ocean. Phys.* **48**(4), 427–431 (2012)
- Bolshakova, A.V., Nosov, M.A.: Parameters of tsunami source versus earthquake magnitude. *Pure Appl. Geophys.* **168**, 2023–2031 (2011). doi:[10.1007/s00024-011-0285-3](https://doi.org/10.1007/s00024-011-0285-3)
- Bolshakova, A.V., Nosov, M.A., Kolesov, S.V.: The properties of co-seismic deformations of the ocean bottom as indicated by the slip-distribution data in tsunamigenic earthquake sources. *Mosc. Univ. Phys. Bull.* **70**(1), 62–67 (2015)
- Chinnery, M.A.: The deformation of ground around surface faults. *Bull. Seism. Soc. Am.* **51**, 355–372 (1961)
- Dotsenko, S.F., Soloviev, S.L.: Mathematical modelling of tsunami excitation processes by slides of the ocean bottom. *Tsunami Res.* (in Russian), 4, 8–20. Moscow (1990a)
- Dotsenko, S.F., Soloviev, S.L.: Comparative analysis of tsunami excitation by “piston” and “membrane” bottom slides. *Tsunami Res.* (in Russian), 4, 21–27 (1990b)
- Ekström, G., Nettles, M., Dziewonski, A.M.: The global CMT project 2004–2010: centroid-moment tensors for 13,017 earthquakes. *Phys. Earth Planet. Int.* **200–201**, 1–9 (2012). doi:[10.1016/j.pepi.2012.04.002](https://doi.org/10.1016/j.pepi.2012.04.002)
- Fujii, Y., Satake, K., Sakai, S.I., Shinohara, M., Kanazawa, T.: Tsunami source of the 2011 off the Pacific coast of Tohoku earthquake. *Earth Planets Space* **63**(7), 815–820 (2011)
- Gusiakov, V.K.: Residual displacements on the surface of an elastic half-space. In: *Conditionally Well-Posed Problems of Mathematical Physics in the Interpretation of Geophysical Observations* (VTs SO RAN, Novosibirsk, 1978), pp. 23–51 (in Russian)
- Gusiakov, V.K.: Relationship of tsunami intensity to source earthquake magnitude as retrieved from historical data. *Pure Appl. Geophys.* **168**, 2033–2041 (2011)
- Gusiakov, V.K.: Strongest tsunamis in the World Ocean and the problem of marine coastal security. *Izv. Atmos. Ocean. Phys.* **50**(5), 435–444 (2014)
- Handbook for tsunami forecast in the Japan sea. Earthquake and Tsunami observation division, seismological and volcanological department, Japan meteorological agency, 22 pp. (2001)
- Hatori, T.: Vertical crustal deformation and tsunami energy. *Bull. Earthq. Res. Inst.* **48**, 171–188 (1970)
- Iida, K.: Magnitude, energy and generation mechanism of tsunamis and a catalogue of earthquakes associated with tsunamis In: *Proceedings of Tsunami Meeting Association 10th Pacific Scientific Congress*, 1961, I.U.G.G. Monograph vol. 24, pp. 7–18 (1963)
- Ito, Y., Tsuji, T., Osada, Y., Kido, M., Inazu, D., Hayashi, Y., Tsushima, H., Hino, R., Fujimoto, H.: Frontal wedge deformation near the source region of the 2011 Tohoku-Oki earthquake. *Geophys. Res. Lett.* **38**, L00G05 (2011). doi:[10.1029/2011GL048355](https://doi.org/10.1029/2011GL048355)
- Ji C (UCSB, Kuril 2006). Rupture process of the 15 November 2006 magnitude 8.3—KURIL island earthquake (Revised), http://earthquake.usgs.gov/earthquakes/eqinthenews/2006/usvcam/finite_fault.php
- Ji, C., Wald, D.J., Helmberger, D.V.: Source description of the 1999 Hector Mine, California earthquake; part I: wavelet domain inversion theory and resolution analysis. *Bull. Seism. Soc. Am.* **92**(4), 1192–1207 (2002)
- Jovanovich, D.B.: An inversion method for estimating the source parameters of seismic and aseismic events from static strain data. *Geophys. J. Astron. Soc.* **43**, 347–365 (1975)

- Kajiura, K.: The leading wave of tsunami. *Bull. Earthq. Res. Inst. Tokyo Univ.* **41**(3), 535–571 (1963)
- Kajiura, K.: Tsunami energy in relation to parameters of the earthquake fault model. *Bull. Earthq. Res. Inst.* **56**, 415–440 (1981)
- Kanamori, H.: Mechanism of tsunami earthquakes. *Phys. Earth Planet Int.* **6**, 346–359 (1972)
- Kanamori, H.: The energy release in great earthquakes. *J. Geophys. Res.* **82**, 2981–2987 (1977)
- Kanamori, H., Anderson, D.L.: Theoretical basis of some empirical relations in seismology. *Bull. Seismol. Soc. Am.* **65**, 1073–1095 (1975)
- Kanamori, H., Brodsky, E.E.: The physics of earthquakes. *Rep. Prog. Phys.* **67**, 1429–1496 (2004)
- Kasahara, K.: *Earthquake Mechanics*, p. 284. Cambridge University Press, Cambridge (1981)
- Kim, D.C., Kim, K.O., Pelinovsky, E., Didenkulova, I., Choi, B.H.: Three-dimensional tsunami runup simulation for the port of Koborinai on the Sanriku coast of Japan. *J. Coast. Res.* **65**, 266–271 (2013)
- Koketsu, K., Yokota, Y., Nishimura, N., Yagi, Y., Miyazaki, S., Satake, K., Fujii, Y., Miyake, H., Sakai, S., Yamanaka, Y., Okada, T.: A unified source model for the 2011 Tohoku earthquake. *Earth Planet. Sci. Lett.* **310**, 480–487 (2011)
- Kurahashi, S., Irikura, K.: Source model for generating strong ground motions during the 2011 off the Pacific coast of Tohoku earthquake. *Earth Planets Space* **63**, 571–576 (2011)
- Laverov, N.P., Lobkovsky, L.I., Levin, B.W., Rabinovich, A.B., Kulikov, E.A., Fine, I.V., Thomson, R.E.: The Kuril tsunamis of 15 November 2006, and 13 January 2007: two trans-pacific events. *Dokl. Earth Sci. MAIK Nauka/Interperiodica* **426**(1), 658–664 (2009)
- Lay, T., Yamazaki, Y., Ammon, C.J., Cheung, K.F., Kanamori, H.: The 2011 Mw 9.0 off the Pacific coast of Tohoku earthquake: comparison of deep-water tsunami signals with finite-fault rupture model predictions. *Earth Planets Space* **63**(7), 797–801 (2011)
- Levin, B.W.: On the nature of some periodic changes in the Earth's seismic regime. *Vestn. Dal'nevost. Otd. Ross. Akad. Nauk* **1**, 51–58 (2006)
- Levin, B.W., Nosov, M.A.: On the possibility of tsunami formation as a result of water discharge into seismic bottom fractures. *Izv. Atmos. Ocean. Phys.* **44**(1), 117–120 (2008)
- Levin, B.W., Sasorova, E.V.: General regularities in the distribution of seismic events on the Earth and on the Moon. *Dokl. Earth Sci.* **434**(1), 1249–1252 (2010)
- Levin, B.W., Sasorova, E.V.: Seismicity of the Pacific: Revealing Global Regularities. *Yanus-K, Moscow* (2012) (in Russian)
- Levin, B.W., Sasorova, E.V.: Spatiotemporal distributions of tsunami sources and discovered periodicities. *Izv. Atmos. Ocean. Phys.* **50**(5), 485–497 (2014). doi:[10.1134/S0001433814050065](https://doi.org/10.1134/S0001433814050065)
- Li, Y., Raichlen, F.: Non-breaking and breaking solitary wave run-up. *J. Fluid Mech.* **456**, 295–318 (2002)
- Maruyama, T.: Statical elastic dislocations in an infinite and semi-infinite medium. *Bull. Earthq. Res. Inst. Tokyo Univ.* **42**, 289–368 (1964)
- Matsu'ura, M., Tanimoto, T.: Quasi-static deformations due to an inclined, rectangular fault in a viscoelastic half-space. *J. Phys. Earth* **28**(1), 103–118 (1980)
- Mikada, H., Mitsuzawa, K., Matsumoto, H., Watanabe, T., Morita, S., Otsuka, R., Sugioka, H., Baba, T., Araki, E., Suyehiro, K.: New discoveries in dynamics of an M8 earthquake—phenomena and their implications from the 2003 Tokachi-Oki earthquake using a long term monitoring cabled observatory. *Tectonophysics* **426**, 95–105 (2006)
- Mogi, K.: Global variation of seismic activity. *Tectonophysics* **57**, 43–50 (1979)
- Newman, A.V., Hayes, G., Wei, Y., Convers, J.: The 25 October 2010 Mentawai tsunami earthquake, from real-time discriminants, finite-fault rupture, and tsunami excitation. *Geophys. Res. Lett.* **38**(5), L01307 (2011)
- Nosov, M.A., Kolesov, S.V.: Method of specification of the initial conditions for numerical tsunami modeling. *Mosc. Univ. Phys. Bull.* **64**(2), 208–213 (2009)
- Nosov, M.A., Kolesov, S.V.: Optimal initial conditions for simulation of seismotectonic tsunamis. *Pure Appl. Geophys.* **168**(6–7), 1223–1237 (2011)

- Nosov, M.A., Nurislamova, G.N.: The potential and vortex traces of a tsunamigenic earthquake in the ocean. *Mosc. Univ. Phys. Bull.* **67**(5), 457–461 (2012)
- Nosov, M.A., Bolshakova, A.V., Kolesov, S.V.: Displaced water volume, potential energy of initial elevation and tsunami intensity: analysis of recent tsunami events. *Pure Appl. Geophys.* **171**, 3515–3525 (2014)
- Nosov, M.A., Kolesov, S.V., Levin, B.W.: Contribution of horizontal deformation of the seafloor into tsunami generation near the coast of Japan on 11 March 2011. *Dokl. Earth Sci.* **441**(1), 1537–1542 (2011). SP MAIK Nauka/Interperiodica
- Nosov, M.A., Kolesov, S.V., Ostroukhova, A.V., Alekseev, A.B., Levin, B.W.: Elastic oscillations of the water layer in a tsunami source. *Dokl. Earth Sci.* **404**(7), 1097–1100 (2005)
- Nosov, M.A., Nurislamova, G.N., Moshenceva, A.V., Kolesov, S.V.: Residual hydrodynamic fields after tsunami generation by an earthquake. *Izv. Atmos. Ocean. Phys.* **50**(5), 520–531 (2014)
- Nostro, C., Piersanti, A., Antonioli, A., Spada, G.: Spherical versus flat models of coseismic and postseismic deformations. *J. Geophys. Res.* **104**(B6), 13,115–13,134 (1999)
- Okada, Y.: Surface deformation due to shear and tensile faults in a half-space. *Bull. Seism. Soc. Am.* **75**(4), 1135–1154 (1985)
- Okada, Y.: Simulated empirical law of coseismic crustal deformation. *J. Phys. Earth* **43**, 697–713 (1995)
- Okal, E.A.: Seismic parameters controlling far-field tsunami amplitudes: a review. *Nat. Hazards* **1**, 67–96 (1988)
- Okal, E.A.: Normal mode energetics for far-field tsunamis generated by dislocations and landslides. *Pure Appl. Geophys.* **160**, 2189–2221 (2003)
- Ozawa, S., Nishimura, T., Suito, H., Kobayashi, T., Tobita, M., Imakiire, T.: Coseismic and postseismic slip of the 2011 magnitude-9 Tohoku-Oki earthquake. *Nature* **475**(7356), 373–376 (2011)
- Pavlov, V.M., Gusev, A.A.: On possibility of motion restoring in the deep earthquake source according to bulk wave field in Fraunhofer region. *Dokl. Akad. Nauk* **255**, 828–834 (1980)
- Pelinovsky, E.N.: *Hydrodynamics of Tsunami Waves* (in Russian). Institute of Applied Physics, RAS, Nizhnii Novgorod (1996)
- Poisson, B., Oliveros, C., Pedreros, R.: Is there a best source model of the Sumatra 2004 earthquake for simulating the consecutive tsunami? *Geophys. J. Int.* **185**(3), 1365–1378 (2011)
- Pollitz, F.F., Bürgmann, R., Banerjee, P.: Geodetic slip model of the 2011M9.0 Tohoku earthquake. *Geophys. Res. Lett.* **38**, L00G08 (2011)
- Poplavskii, A.A., Zolotukhin, D.E., Khramushin, V.N.: A macroseismic model of a tsunami source and estimation of its efficiency by numerical modeling. *J. Volcanol. Seismol.* **6**(1), 58–64 (2012)
- Press, F.: Displacements, strains and tilts at tele-seismic distances. *J. Geophys. Res.* **70**, 2395–2412 (1965)
- Riguzzi, F., Panza, G., Varga, P., Doglioni, C.: Can Earth's rotation and tidal despinning drive plate tectonics? *Tectonophysics* **484**, 60–73 (2010)
- Rhie, J., Dreger, D., Burgmann, R., Romanowicz, B.: Slip of the 2004 Sumatra-Andaman earthquake from joint inversion of long-period global seismic waveforms and GPS static offsets. *Bull. Seism. Soc. Am.* **97**(1A), S115–S127 (2007)
- Satake, K.: Inversion of tsunami waveforms for the estimation of a fault heterogeneity: method and numerical experiments. *J. Phys. Earth* **35**(3), 241–254 (1987)
- Satake, K., Imamura, F.: Tsunamis: seismological and disaster prevention studies. *J. Phys. Earth* **43**(3), 259–277 (1995)
- Satake, K., Tanioka, Y.: Sources of tsunami and tsunamigenic earthquakes in subduction zones. *Pure Appl. Geophys.* **154**, 467–483 (1999)
- Sato, R.: Theoretical basis on relationships between focal parameters and earthquake magnitude. *J. Phys. Earth* **27**, 353–372 (1979)
- Savage, J.C., Hastie, L.M.: Surface deformation associated with dip-slip faulting. *J. Geophys. Res.* **71**, 4897–4904 (1966)

- Shao, G., Li, X., Ji, C., Maeda, T.: Focal mechanism and slip history of the 2011 Mw 9.1 off the Pacific coast of Tohoku earthquake, constrained with teleseismic body and surface waves. *Earth Planets Space* **63**(7), 559–564 (2011)
- Suzuki, W., Aoi, S., Sekiguchi, H., Kunugi, T.: Rupture process of the 2011 Tohoku-Oki mega-thrust earthquake (M9.0) inverted from strong-motion data. *Geophys. Res. Lett.* **38**(7) (2011)
- Tanioka, Y., Satake, K.: Fault parameters of the 1896 Sanriku tsunami earthquake estimated from tsunami numerical modeling. *Geophys. Res. Lett.* **23**(13), 1549–1552 (1996)
- Ward, S.N.: Relationships of tsunami generation and an earthquake source. *J. Phys. Earth* **28**, 441–474 (1980)
- Ward, S.N., Barrientos, S.E.: An inversion for slip distribution and fault shape from geodetic observations of the 1983 Borah Peak, Idaho earthquake. *J. Geophys. Res.* **91**, 4909–4919 (1986). doi:[10.1029/JB091iB05p04909](https://doi.org/10.1029/JB091iB05p04909)
- Watanabe, T., Matsumoto, H., Sugioka, H., Mikada, H., Suyehiro, K., Otsuka, R.: Offshore monitoring system records recent earthquake off Japan's northernmost island. *Eos* **85**(2) (2004)
- Wei, S., Graves, R., Helmberger, D., Avouac, J.P., Jiang, J.: Sources of shaking and flooding during the Tohoku-Oki earthquake: a mixture of rupture styles. *Earth Planet Sci. Lett.* **333–334**, 91–100 (2012)
- Wells, D.L., Coppersmith, K.J.: New empirical relationships among magnitude, rupture length, rupture width, rupture area, and surface displacement. *Bull. Seismol. Soc. Am.* **84**(4), 974–1002 (1994)
- Yagi, Y., Fukahata, Y.: Introduction of uncertainty of Green's function into waveform inversion for seismic source processes. *Geophys. J. Int.* **186**(2), 711–720 (2011)
- Yamashita, T., Sato, R.: Generation of tsunami by a fault model. *J. Phys. Earth* **22**, 415–440 (1974)

<http://www.springer.com/978-3-319-24035-0>

Physics of Tsunamis

Levin, B.W.; Nosov, M.A.

2016, XIII, 388 p. 167 illus., 114 illus. in color.,

Hardcover

ISBN: 978-3-319-24035-0